Modelling the effects of lymph node swelling on T-cell response

Sarah C Johnson[1], Jennifer Frattolin[1], Lowell T. Edgar[1], Mohammad Jafarnejad[2], James E. Moore Jr.[1]*

[1] Department of Bioengineering, Imperial College London, London, United Kingdom

[2] Department of Biomedical Engineering, Johns Hopkins University School of Medicine, Baltimore, MD, USA

* corresponding author

Email: james.moore.jr@imperial.ac.uk

Abstract

Swelling of the lymph nodes is commonly observed during the adaptive immune response, yet its impacts on T cell trafficking and subsequent immune response are not well known. To better understand the effect of macro-scale alterations in the lymph node, we developed an agent-based model of the lymph node paracortex, describing T cell trafficking and response to antigen-presenting dendritic cells alongside swelling-induced changes in T cell recruitment and egress, and regulation of expression of egress-modulating T cell receptor Sphingosine-1-phosphate receptor-1. Validation of the model was achieved with *in-silico* replication of a range of published *in-vivo* and cell culture experiments. Analysis of $CD4^+$ and $CD8^+$ effector T cell response under varying swelling conditions showed that paracortical swelling aided initial T cell activation but could inhibit subsequent effector $CD8^+$ T cell production if swelling occurs too early in the T cell proliferative phase. This was primarily due to changes in effector T cell egress rather than changes in T cell and Dendritic cell interactions. Temporarily extending retention of newly differentiated effector T cells, mediated by Sphingosine-1-phosphate receptor-1 expression, mitigated the effects of early paracortical swelling. These results suggest that targeting the timing of lymph node swelling and temporary effector T cell retention may offer new ways to modulate effector TC responses in for example, immuno-suppressed patients or to optimise vaccine design.

Author summary

Within lymph nodes, interaction of T cells and antigen-presenting cells play a crucial role in initiating the adaptive immune response, resulting in effector T cells that travel to the infection site. Accompanying lymph node swelling is commonly observed, yet the impact on T cell trafficking and subsequent immune response is not well understood. We developed an agent-based lymph node model, describing immune response-induced expansion and changes

in T cell recruitment and egress. We included regulation of T cell expression of Sphingosine-1-phosphate receptor-1 due to the important role in T cell trafficking. We found that although swelling aids T cell activation, too early an increase in paracortical volume can hinder $CD8^+$ effector T cell response. This was primarily due altered in effector T cell egress rather than T cell interactions. Temporary extension of Sphingosine-1-phosphate receptor-1 downregulation on newly differentiated effector T cells greatly increased overall effector T cell output and could counteract loss in effector T cell production due to early swelling. Increased T cell retention during initial lymph node shutdown did not produce the same effect. Our findings suggest targeting the timing of lymph node swelling and temporary effector T cell retention may offer new ways to manipulate immune response.

Introduction

The lymphatic system is a network of organs and lymphatic vessels (LVs) that maintains fluid balance in the body and also delivers crucial antigen information to lymph nodes (LNs) for initiation of adaptive immunity. A successful immune response relies not only on the interaction of different immune cell types, but also on the maintenance of an appropriate physical environment in the LNs to facilitate those interactions. LNs contain specific compartments populated by T cells (TCs), B cells, fibroreticular cells (FRCs), and lymphatic endothelial cells (LECs) [1,2]. When antigens are presented (either suspended in lymph or as captured by incoming antigen presenting cells), the LNs' physical environment changes over time. Swelling of LNs is a well-known consequence of antigen presentation, but the effects of swelling on the processes crucial for adaptive immunity are not well understood.

The mechanism driving LN swelling in response to antigens can be attributed to more than one factor, for example, Dendritic Cell (DCs) presence, B cell signalling and trapping of non-

activated TCs in the LNs [3-6]. During oedema, where peripheral lymphatic fluid accumulates, LN swelling is not routinely observed; therefore, swelling due to increased afferent fluid loading alone is unlikely. Regardless of the trigger, within the first 2 days, TC exit rate falls (sometimes called “LN shutdown”), blood flow to the LN increases, and inflammatory signalling results in a 3-5 fold increase in TC recruitment via high endothelial venules (HEV) [7-10]. LN mass increases 2-5-fold, accompanied by a similar increase in cellularity; in the first 48-96 hours, and the FRCs elongate to accommodate the increase in LN size [6,11,12]. Proliferation of stromal cells lags behind the increase in immune cells, but subsequent proliferation of LECs and FRCs allow maintenance of the LNs architecture during further expansion [5,12,13]. The blood vessels of the LNs also grow, increasing blood vessel volume roughly proportional to the overall volume of the LNs, accompanied by further TC recruitment [4,9,14].

Between 2- and 5-days post-immunisation, the number of antigen-presenting DCs in LNs peaks, TC activation and proliferation is underway and TC egress increases 3-6 fold [5,6,15,16]. Expansion of the medullary and subcapsular sinus (SCS) areas has also been observed, which aids in the increase in TC egress rate [17]. Recruitment of TCs then declines, HEV, FRC and TC proliferation subsides, remaining effector TCs may undergo apoptosis and the LNs return to their baseline volume [14]. Following a primary response, FRC, LEC and blood vessel endothelial cell numbers remain elevated within denser LNs structures for at least one month [13].

To pass through these phases, the underlying antigenic stimulus must be sufficient to trigger lymphocyte retention, activation and proliferation, while a successful immune response occurs when TCs further differentiate into effector cells and migrate out of the LNs [18].

Migrating DCs cross the SCS floor in a chemokine and integrin-aided fashion and migrate into the paracortex [19]. TCs and B Cells mainly enter the LNs by transmigrating from blood vessels in the paracortex [20]. Typically, 1 in 10,000 naïve TCs express a complementary TC receptor to the antigen fragment presented by DCs within a MHCI (to $CD8^+$ TCs) or MHCII ($CD4^+$ TCs) molecule [21,22]. Naive cognate TCs initially make short contacts with DCs, but after around 8 hours, progress to longer interactions (>1hr) before returning to short interactions as TCs activate and divide [23]. With sufficient affinity and stimuli, TCs undergo activation, and secrete inflammatory and activation-facilitating cytokines [24]. Some TCs differentiate into effector TCs and up-regulate the Sphingosine-1-phosphate receptor-1 ($S1P_1r$), facilitating egress [25]. An increasing proportion of TCs differentiate into memory cells [26,27]. Proliferation of $CD8^+$ TCs can continue independent of further stimuli, possibly with an impaired memory cell response [28,29]. Contrastingly, $CD4^+$ TCs are more dependent on sustained inflammatory stimulation for continued differentiation [30]. As infectious signals subside, remaining effector TCs undergo apoptosis while memory cells go into circulation [31].

Throughout these processes, the egress of TCs from the LNs is modulated by Sphingosine-1-Phosphate (S1P) and chemokine signalling axes. After entering the LNs, TCs initially express $S1P_1r$ at very low levels but begin re-expressing $S1P_1r$ after 2 hours [32,33]. TCs exit the LNs by probing and subsequently entering cortical sinuses in the paracortex or the interface with the medulla, aided by chemotaxis as both destinations contain higher S1P concentrations (Fig 1A) [34,35]. During inflammation, TC $S1P_1r$ expression is reciprocally regulated by CD69, an early TC activation marker that can be upregulated in TCs by the presence of inflammatory mediators, contributing to the initial variable decrease of up to 80% in TC egress, termed LN shutdown, and later in the retention of activated TCs [10,36].

Figure 1: Model geometry and structure. (A) LN structure displaying the pathway of arriving lymphatic fluid containing agDCs. (B) The model contains a spherical paracortex. TCs enter in the centre and exit near the interface with the medulla and SCS. The paracortex radius expands as a function of TCs present. (C) At the microscale, TCs move to adjacent grid-compartments (6 of 8 possible movements shown), interact with neighbouring agents and are influenced by the grid-compartment properties, which are updated each time-step. Microscale signals can affect TC recruitment, TC exit and stimulation via interaction with DCs. (D) Interactions between micro and macro scales.

The exploration of potential roles for LN swelling in adaptive immunity is limited by the range of viable experiments that can target specific mechanisms or components while also tracking relevant outcomes in real time. Mathematical models allow time-specific manipulation and tracking of experimentally unobtainable variables, with outcomes helping to fill knowledge gaps and optimise experimental design. We chose to develop a model that could describe both macroscale geometric changes and the microscale TC and DC interactions that drive LN swelling. Agent Based Models (ABMs) can model cells as discrete agents, allowing differing internal states that capture biological variance. By modelling the interaction of thousands of agents following probabilistic rules and behaving individually, it is possible to capture emergent behaviours. ABMs also allow for spatially realistic descriptions of HEV location, afferent lymphatics and TC exit areas into the medullary sinuses. These points are critical for an accurate description of cell transit, as well as for future integration with an antigen and chemokine mass transport model. The FRC network was not incorporated, as previous lattice-based models have shown minimal impact on TC

cell contacts and transit [37-39], and random-walk behaviour of TCs is observed *in-vivo* regardless of stromal cell contribution [40-43].

Several ABMs of fixed-volume LNs have been developed to analyse the influence of the micro-scale signal interaction level. These models have provided insight relevant to vaccine design, for example to investigate the effect of antigenic peptide separation from MHC molecules on TC activation, influential aspects of TC-DC interaction, and effector TC or memory cell production [44-48]. Similar models that include paracortical expansion assume a constant TC occupancy of the total paracortical volume, which may neglect the effects of crowding on TC migration [49-51]. As our focus is on macroscale changes and the resulting physical impact, rather than refining descriptions of intra-cellular signalling cascades, allowing changes in cellular crowding is particularly important due to the potential impact on egress rates and future implementations of pressure and flow. Simulations integrating a fixed-volume hybrid lattice-based model and a continuous model allowed incorporation of chemokine diffusion with TC, B cell and DC interactions in the LNs. This showed that both early antigen removal and regulation of TC exit affected the balanced system dynamics, indicating that macroscale swelling is likely to significantly affect micro-scale TC activity [52]. Indeed, models of lymph flow through the LNs suggest that altered oncotic and medulla pressure alone would dramatically alter cell, cytokine and chemokine distributions [53,54].

In summary, the adaptive immune response involves careful trafficking and coordination of immune cell movements in the LNs, suggesting that swelling of LNs is likely to significantly impact the adaptive response at the micro-scale. To investigate this hypothesis, a computational ABM was developed that incorporates TC and DC dynamics, swelling of LNs and changes in TC recruitment and egress. The model was first validated against available

experimental data. The results suggest an important role for swelling of LNs in TC population dynamics.

Materials and methods

ABM Geometry

The paracortex is modelled as a sphere with an initial radius of R_0=200μm, derived from confocal images [2,55]. To reduce computational expense, geometric symmetry is assumed so that only one-half of the total spherical geometry is modelled. The modelling domain is divided into cuboid grid compartments, with an edge length of 6μm (Fig 1C). For each grid compartment, we track which area of the paracortex is represented, such as 'exit', 'boundary' or 'outside'. Paracortical swelling or contraction is achieved by changing the type of region that each grid compartment represents, while maintaining entry and exit areas defined as a percentage of the outer radius (Fig 2A, Fig A in S1 File). To model swelling, we first collated and assessed information from murine experiments regarding changes in LN mass and volume, TC counts, structural cells counts, migrating DC counts, TC recruitment and TC egress following the application of an antigenic stimulus (Fig 2A) [4,6,7,14,15]. Based on this data, we calculate paracortical volume as a sigmoidal function of TCs present (Fig 2A).

Figure 2: Modelling the changes in paracortical volume, TC recruitment and TC expression of $S1P_1r$. A) Previously published experimental data from studies of multiple influences on LN swelling were used to inform the selection and parameterization of a sigmoidal function to drive LN swelling based on TC numbers. B) TC recruitment is driven by initial antigenic signal (eq. 2), with parameterization based on *in-vivo* data, and a proportional increase due to expansion of HEVs. C) $S1P_1r$ expression mediated the retention

of (i) naïve TCs post-transmigration from the blood, (ii) naïve TCs during LN shutdown and (iii) activated and early effector TCs.

TC recruitment

Under baseline conditions, TC recruitment rate is specified as 2000 TCs/hour, with naive TC transit time (T_{res}) defined between 6-24 hours and the TC-to-compartment ratio assumed constant (1.1 in S1 File). In accordance with HEV images, 90% of TCs enter at 'HEV entry' compartments designated as the inner half of the paracortical radius [56]. The volume of these entry grids also corresponds to the blood vessel volume (V_B), which varies proportionally with the overall change in paracortical volume [4,53]. Remaining TCs enter via the SCS interface at compartments adjacent to the afferent half of the external surface. The TC recruitment rate (T_{in}), is proportional to $\overline{V}_B$, starting with a predefined baseline value. Acute recruitment changes due to inflammation-induced signalling cascades at the HEVs are represented by an inflammatory index, I_F (Eq 1). This index impacts TC influx when the antigenic presence (sum of MHCII) rises above the trigger threshold, T1, the minimal number of DCs required to elicit a response [45]. The value of I_F increases proportionally by a recruitment factor (R_F) with antigenic presence up to a cap threshold, T2, where the maximum inflammation-induced TC recruitment is reached regardless of further stimuli (Eq. 2). TC influx is therefore defined as:

$$T_{in}(t) = \frac{N_T}{T_{res}} I_F(t)\overline{V}_B(t) \quad (1)$$

Where N_T is the initial number of TCs present, T_{res} is the naïve TC transit time, I_F is the inflammatory index, and $\overline{V}_B$ is the normalised blood vessel volume. Threshold values for T1,

T2 and R_F were estimated from TC recruitment rate changes due to inflammation in the initial few days, whilst considering the changes due to HEV growth and agDC number present [6-10,15,57]. The inflammatory index I_F is calculated as:

$$I_F(t) = \begin{cases} 1 & \sum_{n=1}^{N_{DC}} MHC_{II}(t) \leq T1 \\ 1 + R_F \sum_{n=1}^{N_{DC}} MHC_{II}(t) & T1 \leq \sum_{n=1}^{N_{DC}} MHC_{II}(t) \leq T2 \\ 1 + R_F T2 & \sum_{n=1}^{N_{DC}} MHC_{II}(t) \leq T2 \end{cases}$$

(2)

Where Recruitment Factor R_F is the increase in recruitment rate, N_{DC} is the number of agDCs present, and MHC_{II} is the sum of MHCII carried by each agDC.

TC egress and $S1P_1r$ expression

We alter relative TC expression of $S1P_1r$ (SP), from the default value of 1, under three conditions (Fig 2C). Firstly, following TC entry into the paracortex from the blood, $S1P_1r$ remains down-regulated (SP_{in}=0.1) for 45-180 minutes, before re-expressing due to low paracortical S1P concentration [33]. A mechanism of 'LN shutdown' is included by down-regulating $S1P_1r$ (SP_{inflam} = 0.4) on all TCs when antigenic presence is detected. Summation of MHCII present is used as an antigenic signal, set initially to trigger after 6 hours of baseline simulation. Finally, activation-induced TC $S1P_1r$ down-regulation is included by applying the largest decrease in $S1P_1r$ expression when TCs first become activated (SP_{act}=0.01), then increasing $S1P_1r$ expression as TCs differentiate into effector TCs ($SP_{early=}$0.4), and further increasing expression when effector TCs undergo ≥ 8 divisions (SP_{late}=1) [32, 58, 59].

TC and DC motility and interaction

DCs are modelled as 6μm radius spheres. To reflect their long dendrites, DCs can interact with TCs within a two-grid radius, up to a user-defined maximum number of TCs at one time, defined by parameter, B_{max} (Fig A in S1 File). Interaction times are drawn from uniform probability distributions, with brief 3-minute interactions for non-cognate TCs (T_{NC}). Cognate TCs initially undergo short (T_{short}) interactions of 10-15 minutes, then proceed to longer interactions (T_{long}) of 50-70 minutes. Each agDC presents a decaying MHCI and MHCII signal with half-lives $MHCI_{1/2}$ and $MHCII_{1/2}$, obtained from *in-vitro* labelling of MHC molecules presented on DCs [60-63].

TCs are modelled as spheres of volume 150 μm^3 with radius 3.3μm that initially occupy 60% of the total paracortex volume [64]. The starting TC population is composed of 70% helper TCs ($CD4^+$) and 30% cytotoxic TCs ($CD8^+$) [65]. At each timestep (Δt=20s), TCs are permitted to move one grid length to an available neighbouring grid compartment, moving with respect to probability, β, and where availability is governed by crowding parameter, γ. The proportion of cognate TCs recruited each timestep (F_{cog}) was obtained from reported *in-vivo* frequency of antigen-specific TCs [22].

Cognate TCs gain 'stimulation' (***S***) during interactions with agDCs at rate K_s, proportional to MHC presented, while losing stimulation at rate λ_S (Fig A in S1 File), similar to the methods of [46, 50, 66]. The probability of subsequent activation and differentiation is determined as a sigmoidal function of accumulated stimulation. The functions were parameterised such that $CD8^+$ TCs require more accumulated stimulation to activate with the same probability as

$CD4^+$ TCs. However, if the DC is 'licenced', which occurs post-interaction with an activated $CD4^+$ TC, $CD8^+$ TC and $CD4^+$ TC stimulation requirements are equal. This is to reflect facilitated $CD8^+$ activation as a result of activated $CD4^+$ induced production of cytokines [67]. Proliferation is possible every 11 and 9 (+/-1) hours for $CD4^+$ TCs and $CD8^+$ TCs, respectively, while differentiation into effector or memory TCs is only possible after undergoing 4 proliferations [68-71]. A higher level of stimulation is required for $CD4^+$ TCs to differentiate with the same probability as $CD8^+$ TCs. The fraction of effector TCs that differentiate into memory TCs increases from 0.01 to 0.04 as TCs progress from 'early effectors' (< 8 proliferations) to 'late effectors' [72]. See S1 File for full rules and parameter reference Tables A&B.

Computation

The ABM was built in RepastSimphony (http://repast.sourceforge.net) as a class-based model (Fig B in S1 File) written in Java with repeated rules each timestep (Fig 3). Further UML-based descriptions are available within S2 File. The model can be visualised within a GUI (Fig 4). The Imperial College High Performance Computing cluster was used to carry out batch simulations. Data analysis was carried out in Matlab. Complete code is available at github.com/johnsara04/paracortex_model_johnson19.

Figure 3: Structure of the code to set up and run the model. A) The model is initiated in the absence of stimulus, then capacity for paracortical volume change is introduced and variables storing initial starting volumes are updated. Cells (TCs and DCs) are represented by agents that store information about interaction history and present state. The 'Context' describes the environment and 'Projections' between agents allow information transfer. Each

time-step represents 20s and model outputs are recorded every, 1, 15 or 180 time-steps. B) Following equilibration, the 'main' function calls a repeated series of sub-functions that describe DC arrival and TC response. Each function contains further actions, with descriptions available within the supplementary (S2 File).

Figure 4: Model visualization. A) The environment is divided into grid compartments and in this case, the TCs are color-coded based on time spent in the paracortex. B) The grid (cubes with sides of 6μm) is used to distinguish the neighboring areas of cells and cell migration.

Calibration and Validation

Baseline simulations with limited paracortical swelling (V_{max}=1.2) were performed to ensure the baseline parameters (listed in S1 File) produced realistic TC response dynamics. Following calibration, we carried out a series of four simulated experiments varying a single parameter at a time to mimic *in-vivo* and/or *in-vitro* experiments varying the corresponding biological parameter. First, we inhibited the downregulation of $S1P_1r$ on activated TCs *in-silico* and then compared the effects on the total activated and cognate $CD4^+$ and $CD8^+$ TCs present to the effects observed during corresponding *in-vivo* experiments by Lo *et al* and Gräler *et al* [33,73]. Second, we varied the initial proportion of cognate TCs *in-silico* between $1.0x10^{-5}$ and $1.4x10^{-4}$ and compared the resulting $CD4^+$ and $CD8^+$ effector TC response to the relationship between cognition and effector TC number observed in *in-vivo* and *in-vitro* by Obar *et al* and Moon *et al* [72,74]. In the third simulation set, we varied the number of agDCs as a fraction of total TCs (Φ_{DC}) incrementally from 0.04 to 0.0015 (2200 to 77 agDCs). We then compared the CD8+ response *in-silico* to the reported CD8+ effector TC

response found *in-vivo* and *in-vitro* by Kaech *et al*, who injecting mice with varying bacterial antigen dose or agDCs, and by Martín-Fontecha *et al* who applied antigen-pulsed DCs to TC culture [75,76]. Fourth, we simulated early DC apoptosis *in-silico* and compared the effect on the total number of $CD8^+$ effector to the results of Prlic *et al* , whereby agDC lifespan was curtailed in rats by injecting diptheria toxin (DT)-sensitive agDCs into the LNs, then eliminating the DCs with DT injection, prior to natural DC apoptosis [77].

Varying lymph node swelling and TC transit

TC response and changes in TC and DC contacts were analysed while varying maximal fold-increase in swelling volume (V_{Max}) from 1 to 2.8, and while varying the required number of TCs present to reach half of V_{Max} (T_{mid}, Figure 2A) between $8x10^4$ and $13x10^4$. We further investigated the impact of TC retention by modulating $S1P_1r$ expression on newly differentiated TCs (effector TCs having undergone 4-6 proliferations) and varying the initial inflammation-triggered naïve TC retention. To assess the robustness of our primary findings, alternative models were then considered. We compared TC response and changes in TC and DC contacts when modelling paracortical volume as directly proportional to TCs present. We also assessed changes in effector TC response when TCs were permitted to re-enter HEVs, or increased exit probability, if two TCs occupied an exit compartment, and when exit area diameter remained a fixed proportion of the paracortical radius. We used application of ANOVA to detect variance and quantified correlation by calculating Pearson's coefficient. and the R^2 value. A significance threshold of $p<0.05$ was used throughout.

Global sensitivity analysis

To identify any influential but uncertain or biologically unconstrained parameters, we carried out a global sensitivity analysis. A total of 300 parameter combinations were selected using Latin Hypercube sampling to reduce sample size while ensuring inclusion of samples near the minimum and maximum parameter ranges. Simulations using each combination were repeated 3 times. Partial-rank correlation coefficients (PRCCs) between each parameter and output of interest (activated TCs, effector TCs, memory TCs, effector TCs exited and memory TCs exited) were calculated for each day (3-13). This was to quantify the effects of a single parameter while accounting for the effects of other parameters, assuming monotonic relationships [78]. Significance tests were performed between the output PRCCs and zero, meaning weaker correlations may be still be significant [78]. We report all significant PRCCs with strength greater than 0.2 (see S4 File).

Results

The model produces realistic baseline TC motility and response to agDCs

By tracking and recording the TC movement (Fig 5A, B), we confirmed that the calibrated model produced an average TC velocity (n=200) of 13.1μm/min, reaching up to 24μm/min (Fig 5C), in-line with murine *in-vivo* measurements [41,43,56,79,80]. The linear relationship between TC displacement versus square root of time, (Fig 5D, E) illustrated that random walk behaviour was maintained [81]. The motility coefficient (CM), analogous to a diffusion co-efficient, was 63.2μm^2/min, which is within the range of 50-100μm^2/min observed in mice [38]. The mean TC paracortex transit time was 13.1 hours (n=16,000), ranging from 20 minutes to >60 hours (Fig 5F), in-line with observations that 74% of $CD4^+$ TCs and 64% of $CD8^+$ TCs transit murine LNs within a day [82].

Figure 5. Baseline TC motility. A) TC tracking through the paracortex with individual tracks displayed. TCs entered centrally, representing entry from HEVs, and at the top of the paracortex, representing entry in afferent lymph (yellow arrow). TCs exited at the periphery (green arrows). B) Tracks of 200 TCs (each colour represents one TC path) transposed to the same origin point display the random walk behaviour outwards from the origin. C) Most TCs completed transit in <24hrs. D) Mean TC velocity over the entirety of their path. E) Mean and SEM (n=100) of TC displacement from entry point. F) Mean (+/-SEM) of TC displacement showed a linear relationship to the square root of time, indicating that random walk behaviour is maintained.

TC responses to agDC stimuli corresponded well to experimental data from cell-culture models and *in-vivo* trials in mice, sheep and rats, displaying the expected phases of TC trafficking and response (Fig A in S3 File). TC numbers began to increase approximately 6 hours after initial entry of agDCs, and by day 11 had returned to within 15% of pre-stimulus values (Fig 6A), in-line with temporal responses observed *in-vivo* [6,7,15]. The appearance of activated, effector, and memory TCs began at 16-24 hours, day 3.5 and day 5 post-agDC entry, respectively, in agreement with cell-culture models and *in-vivo* observations [83,84]. Effector $CD4^+$ TCs appeared 1-1.5 hours before $CD8^+$ effector TCs (Fig 6A, B). As observed *in-vivo*, the peak population of cognate $CD8^+$ TCs was an order of magnitude higher than that of $CD4^+$ TCs (Fig 6C) [69,85]. The contraction phase began at day 7 and continued through day 11. The increase in TC egress rate peaked a day later than the increase in TC entry rate (Fig 6D), corresponding well with *in-vivo* observations of delayed increase in TC egress and TC recruitment dynamics [11,86].

Figure 6. TC responses in the paracortex following entry of agDCs under baseline conditions. Average result with SEM of 12 simulations. Note the differing vertical scales. Incoming agDCs numbers are depicted by the dot-dashed line in B (right axis). The total number of TCs (black line in A) peaked in the paracortex at 3.5 days and was comprised mainly of non-cognate naïve TCs, as the number of effector TCs (blue line A) peaked at day 6. The appearance of activated TCs (red line in B) began 12 hours after the first agDCs entered. Memory TCs (black line in B) began to appear at 5 days and 25% of the peak number of memory TCs remained at the end of the simulation. Cognate $CD4^+$ TCs (Green line in C) began to proliferate extensively at day 2.2. Cognate $CD8^+$ TCs (purple line C) began to proliferate at day 4 and reached numbers 10x more than cognate $CD4^+$ TCs. D) TC entry rate increased 2x, peaking at day 3, whilst TC egress rate declined between day 1 and 2, then increased 3x by day 4.

Following calibration, the model was validated through replication of *in-vivo* and *in-vitro* experiments

Whilst holding the calibrated parameters, in each of four simulated experiments, a single parameter was varied to mimic published *in-vivo* and *in-vitro* experiments. Abrogating $S1P_1r$ down-regulation after antigenic stimulus detection *in-silico* reduced the number of activated TCs in the paracortex by 60%, 72% and 81% at V_{max}=1.2, 2.0 and 2.5, respectively (Fig 7D). This was a smaller reduction than observed during *in-vivo* experiments when activated TCs maintaining $S1P_1r$ expression were transferred to LNs, resulting in 90% less activated TC retention in the LNs 15 hours later compared to control mice (Fig 7A) [33]. The *in-silico* reduction was, however, greater than the 40% reduction in activated TCs found with constitutive TC expression of $S1P_1r$ *in-vivo* post-immunisation (Fig 7B) [73]. The *in-silico*

total number of $CD4^+$ and $CD8^+$ effector TCs reached 20% and 6% respectively of the control response when $S1P_1r$ was abrogated (Fig 7E, F). This is similar to the 27% and 5% of control response recorded with constitutive inhibition of $S1P_1r$ expression *in-vivo* (Fig 7C) [73]. See Fig B,C & D in S3 File for three additional sets of validation results.

Figure 7. Comparison between in vivo assessments of the effects of $S1P_1r$ downregulation and model predictions. Top row contains experimental data, and bottom row shows comparable modelling results. A. Pre-activated wildtype TCs ($S1P_1r$) and TCs over-expressing $S1P_1r$ ($S1P_1r$++) were transferred into mice and further TC entry was blocked. After 15 hours there was a 90% reduction in retention of $S1P_1r$++ activated TCs. Adapted from Lo *et al* 2005. B) Activated TC number in the LNs 24 hrs post-transfer dropped by 40% in transgenic mice with constitutive $S1P_1r$ expression while (C) proliferative $CD4^+$ and $CD8^+$ TC response decreased to 20% & 6% of that of the wild-type mice. Adapted from Gräler *et al* 1997. D-F). The results of simulations (n=10) preventing $S1P_1r$ downregulation (-SP regulation) compared to baseline simulations (+SP regulation) showed similar trends to these *in-vivo* results (which were not used in model construction). Mean (+-SEM) total activated TCs number was reduced 60%, 72% and 81% at V_{max}=1.2,1.5 & 2. E) The mean (+-SEM) total $CD8^+$ TC number, was diminished to 25,15 and 18% of control response at V_{max}=1.2,1.5 & 2. F) $CD4^+$ TC number was similarly diminished to 8-10% of control at all V_{max} values.

The results of the global parameter sensitivity analysis indicated that the dominant parameters in determining the target outcomes of TC activation, total TC effectors, and TCs exited were F_{cog}, T_{DCin}, V_{max}. The unconstrained parameters used to describe signal integration, such as mean amount of signal accumulated to activate or differentiate, were not identified as

significantly influential ($p>0.05$ and $R^2>0.2$) in determining the target outcomes (see Fig A and Tables A-C in S4 File).

Paracortical swelling consistently aids TC activation but not effector TC production

When maximal swelling (V_{max}) was varied from 1 to 2.8, activated TC number positively correlated with V_{max} ($R^2= 0.96$, $p<10^{-5}$) doubling in number (Fig 8A). However, the total number of effector TCs negatively correlated with V_{max} ($R^2=0.86$, $p<10^{-3}$) and decreased by 15% (Fig 8B). Neither the number of effector TCs that exited by day 10, nor total number of cognate $CD4^+$ TC present, varied significantly (Fig E.ii and E.iii in S3 File). However, total cognate $CD4^+$ TCs that left the paracortex by day 10 increased by 30% and positively correlated with V_{max} ($R^2=0.76$, $p=0.001$) (Fig 8C). Conversely, there was no change in the number of exiting cognate $CD8^+$ TCs with increasing V_{max} (Fig E.iv in S3 File), but the total number of cognate $CD8^+$ TCs present decreased by 25% and negatively correlated with V_{max} ($R^2=0.855$, $p<10^{-3}$) (Fig 8D). The peak rate of TC recruitment positively correlated with V_{max}, and TC egress rate increased with V_{max} from day 3-6 (Fig 8E, F). The pattern of increased TC activation but decreased effector TC production remained when LN volume increased as a linear function of TCs (Fig A in S5 File).

Figure 8. The variation in TC subsets as V_{max} was varied from 1 to 2.8 with $T_{mid}=10^5$. A) The total activated number of TCs in the paracortex incrementally increased with V_{max} and doubled in number between $V_{max}=1$ and 2.8. ($R^2= 0.96$, $p=1.07x10^{-6}$). B) The total number of effector TCs decreased 0.3x with increasing V_{max} ($R^2=0.86$, $p=1.23x10^{-4}$). C) The total number of cognate $CD4^+$ TCs that exited positively correlated with V_{max} ($R^2=0.76$, $p=0.001$) and increased 1.3x. D) The total cognate $CD8^+$ TCs negatively correlated with V_{max}

(R^2=0.855, p=1.28x10^{-4}). E, F) Peak entry and peak exit rate increased proportionally to V_{max}. All results are the mean of n≥7 simulations with SEM displayed.

Varying the ease of swelling influences resulting TC populations

In some cases, varying the required number of TCs present to reach half the maximal swelling (T_{mid}) from a default value of 10^5 counteracted the effect of varying maximal swelling of LNs on effector TC production. Simulations were carried out varying T_{mid} from the default of 10^5 with a lower T_{mid} of 8x10^4 (leading to swelling beginning a day earlier (Fig 9A) or higher T_{mid} of 13x10^4 TCs, alongside a high or low maximal swelling (V_{max}=1.2 or 2.5). We found that, regardless of T_{mid}, at least 40% more activated TCs were recorded when V_{max} was high compared to when V_{max} was low (Fig 9B). At a low T_{mid}, when swelling was increased, there was a significant drop in effector TCs number (Fig 9C). However, at a high T_{mid}, increasing V_{max} no longer negatively impacted effector TC exit. This change in effector TC response was a result of a variation in typical cognate $CD8^+$ TC response. As shown in Fig 8D previously, cognate $CD8^+$ TC number decreased with swelling; this was similarly observed in Fig 9D at a lower T_{mid} of 8x10^4. However, at a higher T_{mid}, cognate $CD8^+$ TC numbers increased with swelling, whereas there was no change associated with T_{mid} in cognate $CD4^+$ TC response (Fig 9E).

When V_{max} was varied in 0.2 increments with a higher T_{mid} of 12x10^4, the number of effector TCs no longer decreased with V_{max} (Fig 9F). An intermediate swelling of 1.8-fold was identified as the optimum V_{max} to produce effector TCs with 7% more total effector TCs recorded than at any other value of V_{max}. Varying both maximal swelling and T_{mid} over a wider range confirmed that swelling size and early swelling increase TC activation, with T_{mid}

correlating negatively with activated TCs at every value of V_{max} (R=0.79-0.99) (Fig E.viii in S3 File). The effect of positive correlation of T_{mid} with effector TCs exited is only clear at larger swelling (V_{max}=2.5) (Fig 9G), which is likely due to the more significant impact of varying T_{mid} with larger swelling (Fig 9A).

Figure 9. Increasing T_{mid} counteracts the loss in effector TCs with V_{max}. Swelling was varied with $T_{mid}=8x10^4$ and $T_{mid}=1.3x10^5$ instead of default (Figure 8). A) The paracortex swells earlier and for a longer duration with a low $T_{mid.}$ B) TC activation increased with larger swelling, but a higher T_{mid} also reduced activation at a large swelling (p=0.002). C) With a lower T_{mid}, as swelling increased, effector TC number decreased. This effect was due to a change in $CD8^+$ TC number (D) as $CD4^+$ TC number (E) increased with V_{max} but was unaffected by varying T_{mid}. F) The results of simulations varying V_{max} in 0.2 increments with a higher T_{mid} of $1.2x10^5$ instead of baseline 10^5, eliminated the negative correlation between effector TCs and swelling. (G) Further simulations varying T_{mid} confirmed that at a large swelling (V_{max}=2.5), delayed swelling with a higher T_{mid} resulted in more total effectors TCs (R^2=0.97,p= $3x10^{-4}$).

Analysis of underlying TC and DC contacts did not identify altered TC and DC contacts as an influential driving mechanism.

We next wanted to better understand whether changes in TC and agDC interactions may be a driving mechanism for changes in effector TC production. When analysing the mean number of interactions with DCs by cognate TCs present at 3 days, there was no trend with swelling (Fig 10A), even when considering the time since the TC entered (Fig 10B). We then instead looked at the mean number of cognate TCs that DCs interacted with over their lifespan. Correlation between swelling and interactions became more significant the later the DCs

entered, beginning from quartile 2, representing DCs that enter at approximately 15-30 hours, (R^2=0.69, p=0.002) to quartile 4 (R^2=0.83, p=2.3x10^{-4}) (Fig 10D). When T_{mid} was increased to 12x10^5 TCs, there was no significant correlation between TC and DC interaction and V_{max} (Fig 10E). When T_{mid} was varied between 8x10^4 and 12x10^4, no significant correlation with the number of interactions with DCs by cognate TCs was found at any swelling value (Fig 10 C), while the number of cognate TCs contacted by DCs showed a positive correlation for DCs in quartile 4 with a large maximal swelling of V_{max} =2.5 only (R^2=0.72, p=0.03) (Figure 10F).

Taken together, these results suggest that the availability of DCs to the cognate TCs is not significantly influenced by the swelling at day 3, a timepoint that corresponds with peak swelling. When swelling was varied and T_{mid} fixed, the DCs that entered during quartile 3 contacted less cognate TCs as V_{max} increased (Fig 10D), but the cognate TCs present did not contact any less DCs at day 3 (Fig 10A). Although during peak swelling time there isn't a clear relationship between contacts and TC response, our model is not constructed such that we can ascertain whether changes in the number of cognate TCs that DCs contact during quartile 4 (day 4-6) are a result of, or contribute to, the increase or decrease in cognate TCs present.

Figure 10. Changes in cognate TCs and agDC interaction with varying swelling. The mean number of interactions with agDCs recorded from cognate TCs present at day 3; (A) showed no trend with swelling, (B) showed no trend with swelling when taking into account the time spent by the TC in the paracortex and (C) showed no trend with T_{mid} when swelling was held constant. The mean number of cognate TCs that a DC interacted with during its lifespan was recorded, and the DCs grouped dependent on entry time (first 25% (Quartile 1) etc. to enter). With default T_{mid} of 10^5 (D), a very weak negative trend with swelling occurred

during Quartile 1 (R^2=0.48, p=0.05), that became stronger the later the DC entered (R^2=0.69, p=0.002; R^2=0.77, p=6.9x10^{-4}; R^2=0.83, p=2.3x10^{-4} for quartile 2, 3 and 4 respectively). (E) With a higher T_{mid} of 1.2x10^5, no clear trend with swelling was identified. F) Only at a large swelling did DCs that entered later (Quartile 4) contact more cognate TCs when increasing T_{mid} (R^2=0.72, p=0.03).

$S1P_1r$-mediated temporary retention of early effector TCs increased TC response.

Regardless of permitted maximal swelling, down-regulating $S1P_1r$ on early effector TCs to less than 80% of naïve TC expression (SP_{Early}<0.8) produced a sustained increase in total TCs, despite the action only directly affecting the small subset of early effector TCs (Fig 11A). We also found that increasing the $S1P_1r$ downregulation by lowering SP_{early} from its default value of 0.4 resulted in changes in effector TC number that far outweighed the changes due to swelling (Fig 11B). SP_{early} inversely correlated with number of effector TCs at every swelling value (R^2=0.92,0.93,0.92, p<0.005). Reducing SP_{early} from 0.4 to 0.05 doubled the number of effectors TCs exiting, while increasing SP_{early} to 0.8 at least halved the number (Fig 11B). When analysing the TC sub-populations, both $CD4^+$ and $CD8^+$ effector TCs that exited the paracortex by day 10 negatively correlated with SP_{early}, and doubled with SP_{early} from 0.4 to 0.05 (Fig 11C, D). This indicates that CD4+ TCs do maintain proliferative capacity under the correct conditions.

Interestingly, the number of TCs contacted by DCs increased with decreasing SP_{early}, but overall decreased with swelling (Fig 11E). Unlike in our previous simulations permitting swelling with default fixed SP_{early} (Fig 10), the effector TC number did not decrease with swelling, suggesting that increased contact is not a driving mechanism. We also took note of the changes in the TC to grid ratio while varying SP_{early} (Fig 11F). With a small V_{max},

increased TC crowding was observed as expected. However, this retention alone did not produce the highest number of effector TCs. Instead, the combination of retention and swelling produced approximately 15% and 10% more effector TCs with V_{max} of 2.0 and 2.5 respectively, outweighing any negative effects of increased TC egress that accompany swelling (Fig 11G). Implementation of an alternative model with non-specific constraint of TC egress by reducing the expansion in the cap-shaped exit area also resulted in increased effector TC exit but prolonged swelling above a 1.4x swelling (Fig B in S5 File).

Figure 11. Temporary retention of effector TCs by modulating $S1P_1r$ expression on newly differentiated TCs (SP_{early}). A) Reducing SP_{early} resulted in a higher total number of TCs in the paracortex. B) Effector TCs that exited the paracortex were influenced more by SP_{early} than by V_{max}, negatively correlating with SP_{early} (R^2>=0.92, p<0.005). SP_{early} negatively correlated with both (C) $CD8^+$ TCs exited (R^2>0.92, p<0.005) and (D) $CD4^+$ TCs exited (R^2>0.91, p<0.005). E). The mean number of cognate TCs contacted increased as SP_{early} was lowered to 0.1 at each value of V_{max} but overall decreased with V_{max}. F) At a smaller maximal swelling, a higher TC to grid ratio was maintained but this did not translate to more or less effector TC production. (G) Reduced SP_{early} resulted in higher overall rates of TC egress in week 2 of the simulation.

Non-specific early LN shutdown with a doubling of LN volume permitted did not significantly impact effector TC production

We also varied the degree of initial LN shutdown (whilst permitting a doubling of LN volume) by downregulating SP_{inflam} from 0.1 (90% downregulation) to SP_{inflam}=1 (no shutdown). Such downregulation could occur in vivo in response to inflammation. As SP_{inflam} decreased, TC activation increased (R^2= 0.83, p=0.01) (Fig 12B), but varying LN

shutdown showed no trend on effector TCs produced (Fig 12C). No correlation between mean number of contacts with DCs by cognate TCs present at day 3 and increased LN-shutdown was observed, but a positive correlation with number of DCs contacted by non-cognate TCs was found (R^2=0.93, p= 0.0017) (Fig 12D). Increasing $S1P_1r$ down-regulation from 60 to 90% resulted in a sharp, 3-fold higher peak in the total number of TCs (Fig 12A) and paracortical volume, which would not be expected physiologically.

Figure 12 Varying LN shutdown by modulating inflammation-induced $S1P_1r$ downregulation (SP_{inflam}). Modulation of $S1P_1r$ down-regulation in response to initial detection of inflammatory signals from no downregulation (SP_{inflam}=1) to 90% downregulation (SP_{inflam}=0.1), A) total TC number decreases several fold but (B) TC activation increases (R^2= 0.83, p=0.01) while (C) Effector TC production shows no trend. D) Non-cognate TCs contact more DCs as SP_{inflam} is increased (R^2=0.93, p=$1.7x10^{-3}$).

Discussion

In this work, we aimed to better understand the role of lymph node swelling and other adaptive immune processes in the formation of TC responses. Our study builds on previous studies that used ABMs to investigate the impact of stimuli, interaction dynamics, signal integration kinetics and TC migration on effector and memory cell generation in the paracortex, with the aim of better understanding how to manipulate immune response [44-46,48,50]. We focused our results analysis on macroscale alterations and accompanying changes in egress and recruitment. The model was calibrated to baseline conditions that produce a TC response comparable to one set of *in-vivo* results and validated by confirming the *in-silico* TC response matched those observed in a combination of separate *in-vivo* and *in-vitro* studies. By varying paracortical swelling and $S1P_1r$ expression, we showed that

paracortical swelling aids TC activation, but early swelling can impair effector TC response. However, temporary retention of newly differentiated TCs influences the overall effector TC response more than swelling, providing a potential mechanism to overcome swelling-related impairment. Analysis of the underlying mechanisms suggest that the changes in egress probability are more influential than alteration in TC and DC contacts.

A key finding was that, although paracortical swelling facilitated activated TC production over a 5-day period, subsequent effector TC numbers only increased with additional non-specific exit constraints or specific early effector TC retention. During swelling, TC trafficking rate is increased with swelling while activated TCs are retained (Fig 8). Increased TC recruitment from HEV implies that more cognate TCs enter, facilitating screening and leading to more TC activation, an effect that is amplified as the activated TCs proliferate [9]. However, we found that increased activation with larger and/or earlier swelling did not consistently lead to more effector TCs. Instead, swelling that occurred too early reduced the total number of effector TCs and the number of effector $CD8^+$ TCs that exited, and without additional $S1P_1r$ retention or constrained exit, swelling only ever reduced or maintained effector TC production (Fig 9, S4 File). Our results also resemble those from *in-vivo* experiments showing that TC activation is depleted with removal of $S1P_1r$-mediated retention, but also that under these conditions, swelling also no longer aids TC activation (Fig 7).

We found that although swelling is well underway by day 3, there was no clear impact on the mean number of interactions with agDCs by cognate TCs (Fig 10). We also found that by day 4.5, the number of cognate TCs that each agDC has interacted with decreased with swelling. Whether this is due to, or contributes to, less cognate TCs present is unclear. By day 6, most

DCs have undergone apoptosis. When alternative models of egress were considered, increased TC activation with swelling could result in increased effector TC production, when the exit area growth with swelling was constrained (Fig B in S5 File). It thus appears that delayed swelling allows for TC recruitment and retention to be a stronger initial influence than TC egress, by reducing access to exit points and thus the egress rate.

Another key finding was that temporary $S1P_1r$-mediated retention of newly differentiated effector TCs could counteract effects due to swelling that resulted in reduced effector TC number (Fig 11). As $S1P_1r$ downregulation decreased, TC and DC contact increased. With swelling, TC and agDC contact decreased but the numbers of exiting effector TC remained constant. This further suggests increased retention has a stronger effect than increased agDC contact. Non-specific retention in the first few days had no impact on effector TC response (Fig 12).

The temporary nature of this modulation at a later timepoint is crucial to increase effector TC number. Therapeutically, down-regulation of TC $S1P_1r$ is currently the mechanism of multiple sclerosis drug Fingolipid to maintain effector TCs in the LN indefinitely [87]. This is to prevent autoimmune response in the brain but also results in reduced lymphocyte numbers in the blood due to a block of TC egress from the thymus. Permanent inhibition of $S1P_1r$ expression on effector TCs only has also been carried out *in-vivo* [25]. However, temporary downregulation on selectively newly differentiated TCs may prove technically difficult, suggesting identification of alternative means of retention is desirable.

We also found that early swelling hindered $CD8^+$ effector TC response more than that of $CD4^+$ TCs (Fig 9). However, increased $S1P_1r$ downregulation by early effector TCs also

increased $CD4^+$ TC production, indicating that the capacity for further $CD4^+$ expansion remained. The earlier and shorter duration of proliferation of $CD4^+$ TCs may mean that further proliferation is proportionally less affected by increases in TC egress that accompany paracortical swelling compared to $CD8^+$ TCs [69].

The insight provided by our results imply chronically inflamed LNs could be addressed by modulating newly-differentiated effector TC egress with swelling through $S1P_1r$ expression, or by manipulating access to exit areas. Physiologically, factors that could be manipulated to alter the effective T_{mid} include stromal cell contraction and proliferation rate, the sensitivity of immune response to antigen signalling, and the sensitivity to accumulated fluid and TCs. Astarita *et al.* 2015 induced swelling by transferring 10^6 cognate TCs directly into murine LNs, whilst also effectively modulating T_{mid} by inducing FRC elongation and inhibiting FRC contraction by manipulating the CLEC-2-podoplanin axis [12]. In contrast to our predictions, subsequent TC proliferative response was enhanced by the facilitated swelling. However, as both *in-silico* and *in-vivo* experiments have shown, proliferative response size is proportional to the starting frequency of cognate TCs, an effect that we also observed in our model [22,72,74] (Fig B in S3 File). We suggest that with an inflated number of initial cognate TCs, the time-point at which swelling of LNs becomes helpful is likely shifted forward. Our model could be falsified experimentally by showing that applying the minimal antigenic stimulation required to elicit an immune response will produce more effector TCs when swelling is facilitated than when swelling is impeded.

The purpose of the global sensitivity analysis was to identify parameters having strong influence on outputs of interest, with the intent of focusing future experimental efforts on their identification. This also aids in moderating conclusions influenced by unidentified

parameters. For the majority of the model parameters, where a relevant biological basis exists, we parameterised the model using data from *in-vivo* studies. For parameters $MHCI_{1/2}$ and $MHCII_{1/2}$ (respective MHC half-lives), estimations were based on *in-vitro* studies but had little influence on our outputs of interest in comparison to other parameters. Unconstrained parameters in the model relate to the signal gain and loss (K_s and γ), the characterization of activation and differentiation probabilities ($Act_{\mu 4+}$, $Act_{\mu 8+}$, $Dif_{\mu 4+}$, $Dif_{\mu 8+}$), TC recruitment and paracortical swelling (S4 File). The sensitivity analysis showed that the parameters populating the activation and probability curves were not highly influential. The influence of signal integration patterns has been the focus of previous modelling studies [46,50,66].

Model robustness was assessed by examining whether the model could replicate a variety of *in-vivo* and/or *in-vitro* experiments. Most scenarios of varying stimuli strength, duration and TC cognition rate correlated well with such experiments. In some cases, slight differences were observed, for example, the effect of *in-silico* elimination of agDCs after 12 hours more closely matched *in-vivo* elimination of DCs after 1 hour (Fig C in S3 File). This is possibly because, although the majority of DCs are eliminated rapidly post-DT injection, complete removal of DCs *in-vivo* required additional time (12 hours) [75]. Prevention of $S1P_1r$ downregulation on activated TCs *in-silico* resulted in a smaller reduction in activated TC number (60-80%) than the 90% described by Lo *et al.* 2004, but more than the 40% reported by Gräler *et al.* 1997 (Fig 7) [33,73].

Our model captures both macroscale and microscale interactions, but limitations remain, including the use of a simplified LN geometry, lack of chemotactic influences, and no direct representation of the FRC network. TCs display a random walk regardless of FRC network presence, and previous models suggest TC contacts are not significantly influenced by its

inclusion [37-43]. The fidelity of the model is also limited by a lack of information on the effects of swelling on the availability of medullary exit points. TCs may enter the medulla via specialised junctions at specific fixed 'hotspots' or at cell junctions throughout the tissue [35]. Our model has identified this as an important area for future investigation. We omitted DC migration, but our results indicate that DC availability is not a limiting factor.

Lack of a precise mechanism to drive LN swelling is also a challenge, but use of a sigmoidal function to dictate paracortical volume captured the typical phases of swelling better than alternative models (S4 File). An initial TC increase is permitted without triggering significant swelling, reflecting initial inhibition of stromal cell proliferation by increased secretion of IFN type 1 [88]. The delayed increase in volume in response to TC number then represents the switch in signalling at day 2 to favour LEC proliferation and expansion of LNs, through mechanisms such as DC-induced secretion of VEGF from stromal cells and increased elasticity of FRC network [6,89]. We have also neglected the role of chemokines in retaining TCs [18]. When both CCR7 and $S1P_1r$ expression on TCs is inhibited *in-vivo*, TCs migrate to the edges of the paracortex but cannot exit due to lack of $S1P_1r$ expression [25]. Accordingly, inclusion of $S1P_1r$ down-regulation was prioritised over CCR7, but the strong influence of retention suggests future models should include a wider range of retentive influences [58].

In future model iterations, inclusion of additional factors, such as lymph flow and pressure alterations (along with fluid exchange with nodal blood vessels), could also significantly improve the representation of swelling, and thus TC egress and retention. It has been well-established that changes in hydrostatic and oncotic pressure differences across nodal blood vessel walls can reverse the net fluid exchange [90,91]. Afferent lymphatic flow to the LNs also increases with immune response. Therefore, a key next step is to couple the ABM to a

computational flow model, with resident DCs in the LNs also added, and the maximal permitted swelling increased to confirm the observed trends. Lymph flow also influences chemokine concentration fields, and likely mechanoresponsive cell expression of signalling molecules and receptors.

Conclusion

Our results suggest that, although swelling of LNs may aid TC activation, avoiding excessive swelling of LNs and/or temporary retention of effector TCs may boost effector TC response when initial TC response is small, for example, in immuno-suppressed patients, or desirable, such as when optimizing vaccine design to minimise antigen dose. Our model has proved a useful tool to identify the importance of better understanding alterations in TC egress with swelling. Moreover, retention of newly differentiated TCs via the modulation of the TC receptor Sphingosine-1-phosphate-1-receptor ($S1P_1r$) showed that selective modulation on the small subset of effector TCs could strongly impact the efficiency of TC response, and even overcome loss in efficiency of TC response due to early enlargement. Although permanent blockade of effector TC egress has been utilised to treat multiple sclerosis, temporary retention of effector TCs to boost subsequent effector TC production presents as a novel mechanism. This finding also emphasizes the influence that retentive features, including factors such as chemokines, may have on effector TC response, which may be more practical *in-vivo* targets to manipulate.

Acknowledgements

The authors gratefully acknowledge the assistance provided by Dr Samira Jamalian and Willy Bonneuil.

References

1. Chang JE, Turley SJ. Stromal infrastructure of the lymph node and coordination of immunity. Trends in Immunology. 2014;36(1):30–39.
2. Mueller SN, Germain RN. Stromal cell contributions to the homeostasis and functionality of the immune system. Nature Reviews Immunology. 2009;9:618–29.
3. Chyou S, Benahmed F, Chen J, Kumar V, Tian S, Lipp M, et al. Coordinated regulation of lymph node vascular-stromal growth first by CD11c+ cells and then by T and B cells. Journal of immunology. 2011;187(11):5558–67. doi:10.4049/jimmunol.1101724.
4. Kumar V, Scandella E, Danuser R, Onder L, Nitschké M, Fukui Y, et al. Global lymphoid tissue remodeling during a viral infection is orchestrated by a B cell–lymphotoxin-dependent pathway. Blood. 2010;115(23):4725–4733. doi:10.1182/blood-2009-10-250118.
5. Yang CYY, Vogt TK, Favre S, Scarpellino L, Huang HYY, Tacchini-Cottier F, et al. Trapping of naive lymphocytes triggers rapid growth and remodeling of the fibroblast network in reactive murine lymph nodes. PNAS. 2014;111(1):E109–18. doi:10.1073/pnas.1312585111.
6. Acton SE, Farrugia AJ, Astarita JL, Mourao-Sa D, Jenkins RP, Nye E, et al. Dendritic cells control fibroblastic reticular network tension and lymph node expansion. Nature. 2014;514(7523):498–502.
7. Tedla N, Wang H, HP M. Regulation of T lymphocyte trafficking into lymph nodes during an immune response by the chemokines macrophage inflammatory protein (MIP)-1 and MIP-1I2. The Journal of Imm. 1998;161(10):5663–72.

8. Hay JB, Hobbs BB. The flow of blood to lymph nodes and its relation to lymphocyte traffic and the immune response. Journal of Experimental Medicine. 1977;145(1):31–44.
9. Soderberg KA, Payne GW, Sato A, Medzhitov R, Segal SS, Iwasaki A. Innate control of adaptive immunity via remodeling of lymph node feed arteriole. Proceedings of the National Academy of Sciences of the United States of America. 2005;102(45):16315–16320. doi:10.1073/pnas.0506190102.
10. Cahill R, Frost H, Trnka Z. The effects of antigen on the migration of recirculating lymphocytes through single lymph nodes. J Exp Med. 1976;143(4):870–888. doi:10.1084/jem.143.4.870.
11. Drayson MT, Smith ME. The sequence of changes in blood flow and lymphocyte influx to stimulated rat lymph nodes. Immunology. 1981;44:125–133.
12. Astarita JL, Cremasco V, Fu J, Darnell MC, Peck JR, Nieves-Bonilla JM, et al. The CLEC-2-podoplanin axis controls fibroblastic reticular cell contractility and lymph node microarchitecture. Nature Imm. 2015;16(1):75–84.
13. Gregory JL, Walter A, Alexandre YO, Hor JL, Liu R, Ma JZ, et al. Infection Programs Sustained Lymphoid Stromal Cell Responses and Shapes Lymph Node Remodeling upon Secondary Challenge. Cell Reports. 2017;18(2):406 – 418. doi:https://doi.org/10.1016/j.celrep.2016.12.038.
14. Kumar V, Chyou S, Stein J, Lu T. Optical projection tomography reveals dynamics of HEV growth after immunization with protein plus CFA and features shared with HEVs in acute. Frontiers in immunology. 2012;7(3):282.
15. Webster B, Ekland EH, Agle LM, Chyou S, Ruggieri R, Lu TT. Regulation of lymph node vascular growth by dendritic cells. J Exp Med. 2006;203(8):1903–13. doi:10.1084/jem.20052272.

16. Tzeng TC, Chyou S, Tian S, Webster B, Carpenter AC, Guaiquil VH, et al. CD11chi Dendritic Cells Regulate the Re-establishment of Vascular Quiescence and Stabilization after Immune Stimulation of Lymph Nodes. The Journal of Immunology. 2010;184(8):4247–4257. doi:10.4049/jimmunol.0902914.
17. Tan KW, Yeo KP, Wong FHS, Lim HY, Khoo KL, Abastado JP, et al. Expansion of Cortical and Medullary Sinuses Restrains Lymph Node Hypertrophy during Prolonged Inflammation. The Journal of Immunology. 2012;188(8):4065–4080. doi:10.4049/jimmunol.1101854.
18. Cyster JG. Chemokines, sphingosine-1-phosphate, and cell migration in secondary lymphoid organs. Annu Rev Immunol. 2005;23:127–59. doi:10.1146/annurev.immunol.23.021704.115628.
19. Braun A, Worbs T, Moschovakis G, Halle S, Hoffmann K, Bölter J, et al. Afferent lymph-derived T cells and DCs use different chemokine receptor CCR7-dependent routes for entry into the lymph node and intranodal migration. Nat Immunol. 2011;12(9):879–87. doi:10.1038/ni.2085.
20. von Andrian UH, Mempel TR. Homing and cellular traffic in lymph nodes. Nature reviews Immunology. 2003;3(11):867–78. doi:10.1038/nri1222.
21. Blattman JN, Antia R, Sourdive DJ, Wang X, Kaech SM, Murali-Krishna K, et al. Estimating the Precursor Frequency of Naive Antigen-specific CD8 T Cells. The Journal of Experimental Medicine. 2002;195(5):657–664.
22. Jenkins MK, Moon JJ. The role of naïve T cell precursor frequency and recruitment in dictating immune response magnitude. Journal of Immunology (Baltimore, Md : 1950). 2012;188(9):4135–4140.
23. Bousso P. T-cell activation by dendritic cells in the lymph node: lessons from the movies. Nature Reviews Immunology. 2008;8:675–84.

24. Pennock ND, White JT, Cross EW, Cheney EE, Tamburini BA, Kedl RM. T cell responses: naïve to memory and everything in between. Advances in Physiology Education. 2013;37(4):273–283.
25. Benechet AP, Menon M, Xu D, Samji T, Maher L, Murooka TT, et al. T cell-intrinsic S1PR1 regulates endogenous effector T-cell egress dynamics from lymph nodes during infection. PNAS. 2016;113(8):2182–2187. doi:10.1073/pnas.1516485113.
26. Youngblood B, Hale JS, Kissick HT, Ahn E, Xu X, Wieland A, et al. Effector CD8 T cells dedifferentiate into long-lived memory cells. Nature. 2017;552(7685):404–9.
27. Wherry EJ, Ahmed R. Memory CD8 T-Cell Differentiation during Viral Infection. Journal of Virology. 2004;78(11):5535–5545. doi:10.1128/JVI.78.11.5535-5545.2004.
28. van Stipdonk MJB, Lemmens EE, Schoenberger SP. Naïve CTLs require a single brief period of antigenic stimulation for clonal expansion and differentiation. Nature Immunology. 2001;2:423–9.
29. Bevan MJ. Helping the CD8+ T-cell response. Nature Reviews Immunology. 2004;4:595–602.
30. Schrum AG, Palmer E, Turka LA. Distinct temporal programming of naive CD4(+) T cells for cell division versus TCR-dependent death susceptibility by antigen-presenting macrophages. European journal of immunology. 2005;35(2):449–459.
31. Parijs LV, Abbas AK. Homeostasis and Self-Tolerance in the Immune System: Turning Lymphocytes off. Science. 1998;280(5361):243–248. doi:10.1126/science.280.5361.243.
32. Matloubian M, Lo C, Cinamon G, Lesneski M, Xu Y. Lymphocyte egress from thymus and peripheral lymphoid organs is dependent on S1P receptor 1. Nature. 2004;427(6972):355–60. doi:10.1038/nature02284.

33. Lo C, Xu Y, Proia R, Cyster J. Cyclical modulation of sphingosine-1-phosphate receptor 1 surface expression during lymphocyte recirculation and relationship to lymphoid organ transit. Journal of Experimental Medicine. 2005;2(201):291–301. doi:10.1084/jem.20041509.

34. Cyster J, Schwab S. Sphingosine-1-phosphate and lymphocyte egress from lymphoid organs. Annual review of immunology. 2012;30:69–94. doi:10.1146/annurev-immunol-020711-075011.

35. Grigorova I, Schwab S, Phan T, Pham T. Cortical sinus probing, S1P1-dependent entry and flow-based capture of egressing T cells. Nature Imm. 2009;10:58–65. doi:10.1038/ni.1682.

36. Hunter M, Teijeira A, Halin C. T cell trafficking through lymphatic vessels. Frontiers in Immunology. 2016;7:613.

37. Novkovic M, Onder L, Cupovic J, Abe J, Bomze D, Cremasco V, et al. Topological Small-World Organization of the Fibroblastic Reticular Cell Network Determines Lymph Node Functionality. PLOS Biology. 2016;14(7):1–20. doi:10.1371/journal.pbio.1002515.

38. Beltman JB, Marée AFM, Lynch JN, Miller MJ, de Boer RJ. Lymph node topology dictates T cell migration behavior. Journal of Experimental Medicine. 2007;204(4):771–780. doi:10.1084/jem.20061278.

39. Graw F, Regoes RR. Influence of the Fibroblastic Reticular Network on Cell-Cell Interactions in Lymphoid Organs. PLOS Computational Biology. 2012;8(3):1–9. doi:10.1371/journal.pcbi.1002436.

40. Miller MJ, Hejazi AS, Wei SH, Cahalan MD, Parker I. T cell repertoire scanning is promoted by dynamic dendritic cell behavior and random T cell motility in the lymph

node. Proc Natl Acad Sci USA. 2004;101(4):998–1003. doi:10.1073/pnas.0306407101.

41. Miller MJ, Wei SH, Parker I, Cahalan MD. Two-photon imaging of lymphocyte motility and antigen response in intact lymph node. Science. 2002;296(5574):1869–73. doi:10.1126/science.1070051.
42. Bousso P, Robey E. Dynamics of CD8+ T cell priming by dendritic cells in intact lymph nodes. Nature immunology. 2003;4:579–585.
43. Park E, Peixoto A, Imai Y, Goodarzi A, Cheng G. Distinct roles for LFA-1 affinity regulation during T-cell adhesion, diapedesis, and interstitial migration in lymph nodes. Blood. 2010;115(8):1572–81.
44. Brown LV, Gaffney EA, Wagg J, Coles MC. An *in silico* model of cytotoxic T-lymphocyte activation in the lymph node following short peptide vaccination. Journal of the Royal Society, Interface. 2018;15(140):2018.0041.
45. Celli S, Day M, Müller AJ, Molina-Paris C, Lythe G, Bousso P. How many dendritic cells are required to initiate a T-cell response? Blood. 2012;120(19):3945–3948. doi:10.1182/blood-2012-01-408260.
46. Gong C, Mattila JT, Miller M, Flynn JL, Linderman JJ, Kirschner D. Predicting lymph node output efficiency using systems biology. Journal of Theoretical Biology. 2013;335:169–184.
47. Gong C, Linderman J, Kirschner D. Harnessing the Heterogeneity of T Cell Differentiation Fate to Fine-Tune Generation of Effector and Memory T Cells. Frontiers in Immunology. 2014;5:57. doi:10.3389/fimmu.2014.00057.
48. Ziraldo C, Gong C, Kirschner DE, Linderman JJ. Strategic Priming with Multiple Antigens can Yield Memory Cell Phenotypes Optimized for Infection with

Mycobacterium tuberculosis: A Computational Study. Frontiers in Microbiology. 2015;6. doi:10.3389/fmicb.2015.01477.

49. Bogle G, Dunbar PR. Simulating T-cell motility in the lymph node paracortex with a packed lattice geometry. Imm Cell Biol. 2008;86(8):676–687.
50. Bogle G, Dunbar PR. Agent-based simulation of T-cell activation and proliferation within a lymph node. Imm Cell Biol. 2009;88(2):172–179.
51. Bogle G, Dunbar PR. On-lattice simulation of T cell motility, chemotaxis, and trafficking in the lymph node paracortex. PloS one. 2012;7(9):e45258.
52. Baldazzi V, Paci P, Bernaschi M, Castiglione F. Modeling lymphocyte homing and encounters in lymph nodes. BMC Bioinformatics. 2009;10:387. doi:10.1186/1471-2105-10-387.
53. Jafarnejad M, Woodruff MC, Zawieja DC, Carroll MC, Moore J. Modeling Lymph Flow and Fluid Exchange with Blood Vessels in Lymph Nodes. Lymphat Res Biol. 2015;13(4):234–247. doi:10.1089/lrb.2015.0028.
54. Jafarnejad M, Zawieja DC, Brook BS, Nibbs RJB, Moore JE. A Novel Computational Model Predicts Key Regulators of Chemokine Gradient Formation in Lymph Nodes and Site-Specific Roles for CCL19 and ACKR4. The Journal of Immunology. 2017;199(7):2291–2304. doi:10.4049/jimmunol.1700377.
55. Kuka M, Iannacone M. The role of lymph node sinus macrophages in host defense. Annals of the New York Academy of Sciences. 2014;1319(1):38–46. doi:10.1111/nyas.12387.
56. Girard JP, Moussion C, Förster R. HEVs, lymphatics and homeostatic immune cell trafficking in lymph nodes. Nat Rev Immunol. 2012;12(11):762–73. doi:10.1038/nri3298.

57. Mackay C, Marston W, Dudler L. Altered patterns of T cell migration through lymph nodes and skin following antigen challenge. European journal of Imm. 1992;22(9):2205–10. doi:10.1002/eji.1830220904.

58. Pham T, Okada T, Matloubian M, Lo C, Cyster J. S1P 1 receptor signaling overrides retention mediated by Gi-coupled receptors to promote T cell egress. Immunity. 2008;28(1):122–133.

59. Garris CS, Blaho VA, Hla T, Han MH. Sphingosine-1-phosphate receptor 1 signalling in T cells: trafficking and beyond. Immunology. 2014;142(3):347–353.

60. Cella M, Salio M, Sakakibara Y, Langen H, Julkunen I, Lanzavecchia A. Maturation, Activation, and Protection of Dendritic Cells Induced by Double-stranded RNA. The Journal of Experimental Medicine. 1999;189(5):821–829.

61. Kukutsch NA, Rossner S, Austyn JM, Schuler G, Lutz MB. Formation and Kinetics of MHC Class I-Ovalbumin Peptide Complexes on Immature and Mature Murine Dendritic Cells. Journal of Investigative Dermatology. 2000;115(3):449 – 453. doi.org/10.1046/j.1523-1747.2000.00084.x.

62. Cella M, Engering A, Pinet V, Pieters J, Lanzavecchia A. Inflammatory stimuli induce accumulation of MHC class II complexes on dendritic cells. Nature. 1997;388:782–7.

63. Baumgartner C, Ferrante A, Nagaoka M, Gorski J, Malherbe LP. Peptide-MHC Class II Complex Stability Governs CD4 T Cell Clonal Selection. Journal of immunology (Baltimore, Md : 1950). 2010;184(2):573–581.

64. Tasnim H, Fricke GM, Byrum JR, Sotiris JO, Cannon JL, Moses ME. Quantitative Measurement of Näıve T Cell Association With Dendritic Cells, FRCs, and Blood Vessels in Lymph Nodes. Frontiers in Immunology. 2018;9:1571. doi:10.3389/fimmu.2018.01571.

65. Latif R, de Rosbo NK, Amarant T, Rappuoli R, Sappler G, Ben-Nun A. Reversal of the $CD4^+/CD8^+$ T-Cell Ratio in Lymph Node Cells upon In Vitro Mitogenic Stimulation by Highly Purified, Water-Soluble S3-S4 Dimer of Pertussis Toxin. Infection and Immunity. 2001;69(5):3073–3081. doi:10.1128/IAI.69.5.3073-3081.2001.

66. Linderman JJ, Riggs T, Pande M, Miller M, Marino S, Kirschner DE. Characterizing the Dynamics of $CD4^+$ T Cell Priming within a Lymph Node. The Journal of Immunology. 2010;184(6):2873–2885. doi:10.4049/jimmunol.0903117.

67. Smith CM, Wilson NS, Waithman J, Villadangos JA, Carbone FR, Heath WR, et al. Cognate $CD4^+$ T cell licensing of dendritic cells in $CD8^+$ T cell immunity. Nature Immunology. 2004;5:1143–8.

68. De Boer RJ, Homann D, Perelson AS. Different Dynamics of $CD4^+$ and $CD8^+$ T Cell Responses During and After Acute Lymphocytic Choriomeningitis Virus Infection. The Journal of Immunology. 2003;171(8):3928–3935. doi:10.4049/jimmunol.171.8.3928.

69. Foulds KE, Zenewicz LA, Shedlock DJ, Jiang J, Troy AE, Shen H. Cutting Edge: CD4 and CD8 T Cells Are Intrinsically Different in Their Proliferative Responses. The Journal of Immunology. 2002;168(4):1528–1532. doi:10.4049/jimmunol.168.4.1528.

70. Nelson RW, Beisang D, Tubo NJ, Dileepan T, Wiesner DL, Nielsen K, et al. T cell receptor cross-reactivity between similar foreign and self peptides influences naïve cell population size and autoimmunity. Immunity. 2015;42(1):95–107.

71. Tubo NJ, Pagán AJ, Taylor JJ, Nelson RW, Linehan JL, Ertelt JM, et al. Single Naive CD4+ T Cells from a Diverse Repertoire Produce Different Effector Cell Types during Infection. Cell. 2013;153(4):785–796.

72. Obar JJ, Khanna KM, Lefran¸cois L. Endogenous naive $CD8^+$ T cell precursor frequency regulates primary and memory responses to infection. Immunity. 2008;28(6):859–869. doi:10.1016/j.immuni.2008.04.010.

73. Gräler MH, Huang MC, Watson S, Goetzl EJ. Immunological Effects of Transgenic Constitutive Expression of the Type 1 Sphingosine 1-Phosphate Receptor by Mouse Lymphocytes. The Journal of Immunology. 2005;174(4):1997–2003. doi:10.4049/jimmunol.174.4.1997.

74. Moon JJ, Chu HH, Pepper M, McSorley SJ, Jameson SC, Kedl RM, et al. Naive $CD4^+$ T cell frequency varies for different epitopes and predicts repertoire diversity and response magnitude. Immunity. 2007;27(2):203–213.

75. Kaech SM, Ahmed R. Memory $CD8^+$ T cell differentiation: initial antigen encounter triggers a developmental program in naïve cells. Nature Immunology. 2001;2:415–22.

76. Martín-Fontecha A, Sebastiani S, Höpken UE, Uguccioni M, Lipp M, Lanzavecchia A, et al. Regulation of Dendritic Cell Migration to the Draining Lymph Node. Journal of Experimental Medicine. 2003;198(4):615–621. doi:10.1084/jem.20030448.

77. Prlic M, Hernandez-Hoyos G, Bevan MJ. Duration of the initial TCR stimulus controls the magnitude but not functionality of the CD8+ T cell response. Journal of Experimental Medicine. 2006;203(9):2135–2143. doi:10.1084/jem.20060928.

78. Marino S, Hogue IB, Ray CJ, Kirschner DE. A methodology for performing global uncertainty and sensitivity analysis in systems biology. Journal of Theoretical Biology. 2008;254(1):178–196. doi:https://doi.org/10.1016/j.jtbi.2008.04.011

79. Boscacci R, Pfeiffer F, Gollmer K, Sevilla A. Comprehensive analysis of lymph node stroma-expressed Ig superfamily members reveals redundant and nonredundant roles for ICAM-1, ICAM-2, and VCAM-1 in lymphocyte homing. Blood. 2010;116(6):915–25.

80. Park C, Hwang I, Sinha R, Kamenyeva O. Lymph node B lymphocyte trafficking is constrained by anatomy and highly dependent upon chemo-attractant desensitization. Blood. 2012;119(4):978–989.

81. Sumen C, Mempel R, Mazo I, von Andrian U. Intravital Microscopy: Visualizing Immunity in Context. Immunity. 2004;21(3):315–329.

82. Tomura M, Yoshida N, Tanaka J. Monitoring cellular movement in vivo with photoconvertible fluorescence protein 'Kaede' transgenic mice. PNAS. 2008;105(31):10871–6. doi:10.1073/pnas.0802278105.

83. Hugues S, Fetler L, Bonifaz L, Helft J, Amblard F, Amigorena S. Distinct T cell dynamics in lymph nodes during the induction of tolerance and immunity. Nature Immunology. 2004;5:1235–42.

84. Kinjyo I, Qin J, Tan SY, Wellard CJ, Mrass P, Ritchie W, et al. Real-time tracking of cell cycle progression during $CD8^+$ effector and memory T-cell differentiation. Nature Communications. 2015;6:6301.

85. Homann D, Teyton L, Oldstone MBA. Differential regulation of antiviral T-cell immunity results in stable $CD8^+$ but declining $CD4^+$ T-cell memory. Nature Medicine. 2001;7(8):913–919.

86. Hall J, Morris B. The immediate effect of antigens on the cell output of a lymph node. British journal of experimental pathology. 1965;46(4):450–454.

87. Chun J, Hartung HP. Mechanism of action of oral fingolimod (FTY720) in multiple sclerosis. Clinical neuropharmacology. 2010;33(2):91–101.

88. Lucas ED, Finlon JM, Burchill MA, McCarthy MK, Morrison TE, Colpitts TM, et al. Type 1 IFN and PD-L1 Coordinate Lymphatic Endothelial Cell Expansion and Contraction during an Inflammatory Immune Response. The Journal of Immunology. 2018;201(6):1735–1747. doi:10.4049/jimmunol.1800271.

89. Lucas ED, Tamburini BAJ. Lymph Node Lymphatic Endothelial Cell Expansion and Contraction and the Programming of the Immune Response. Frontiers in Immunology. 2019;10:36. doi:10.3389/fimmu.2019.00036.

90. Adair TH, Guyton AC. Modification of lymph by lymph nodes. II. Effect of increased lymph node venous blood pressure. American Journal of Physiology-Heart and Circulatory Physiology. 1983;245(4):H616–H622. doi:10.1152/ajpheart.1983.245.4.H616.

91. Adair T, Guyton A. Modification of lymph by lymph nodes. III. Effect of increased lymph hydrostatic pressure. The American journal of physiology. 1985;249:H777–82. doi:10.1152/ajpheart.1985.249.4.H777.

Supporting Information

S1 File. Supplementary Methods A. Further description of modelling methods. 1.1 TC recruitment, 1.2 Agents and agent migration, 1.3 Agent interaction and signal integration. Fig A & B, and parameter Tables A & B.

S2 File. Supplementary Methods B. UML diagrams.

S3 File. Supplementary Results A. Supplementary model calibration (Fig A), model validation (Fig B-D) and LN swelling results (Fig E).

S4 File. Supplementary Results B. Global sensitivity analysis results. Fig A & Tables A-C. The sensitivity of output activated, effector and memory TCs present and effector and memory TCs exited to parameters over the time course of the simulation.

S5 File. Supplementary Results C. Alternative models. 5.1 & Fig A. Consideration of an alternative model with linear TC to LN volume relationship. 5.2 & Fig B. Considering alternative models of TC crowding and egress.

Fig 1. Model geometry and structure. (A) LN structure displaying the pathway of arriving lymphatic fluid containing agDCs. (B) The model contains a spherical paracortex. TCs enter in the centre and exit near the interface with the medulla and SCS. The paracortex radius expands as a function of TCs present. (C) At the microscale, TCs move to adjacent grid-compartments (6 of 8 possible movements shown), interact with neighbouring agents and are influenced by the grid-compartment properties, which are updated each time-step. Microscale signals can affect TC recruitment, TC exit and stimulation via interaction with DCs. (D) Interactions between micro and macro scales.

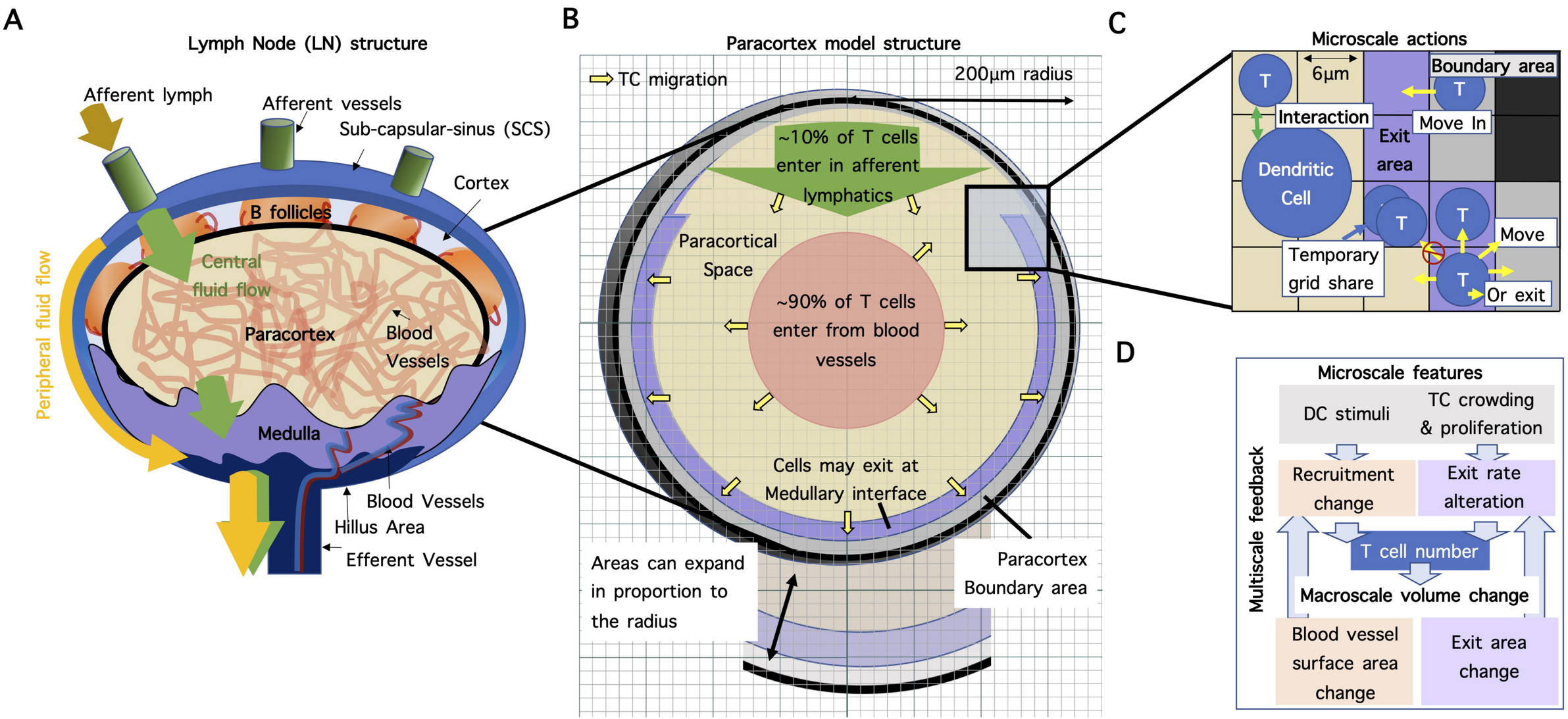

Figure 2. Modelling the changes in paracortical volume, TC recruitment and TC expression of $S1P_1r$. A) Previously published experimental data from studies of multiple influences on LN swelling were used to inform the selection and parameterisation of a sigmoidal function to drive LN swelling based on TC numbers. B) TC recruitment is driven by initial antigenic signal (eq. 2), with parameterization based on *in-vivo* data, and a proportional increase due to expansion of HEVs. C) $S1P_1r$ expression mediated the retention of (i) naïve TCs post-transmigration from the blood, (ii) naïve TCs during LN shutdown and (iii) activated and early effector TCs.

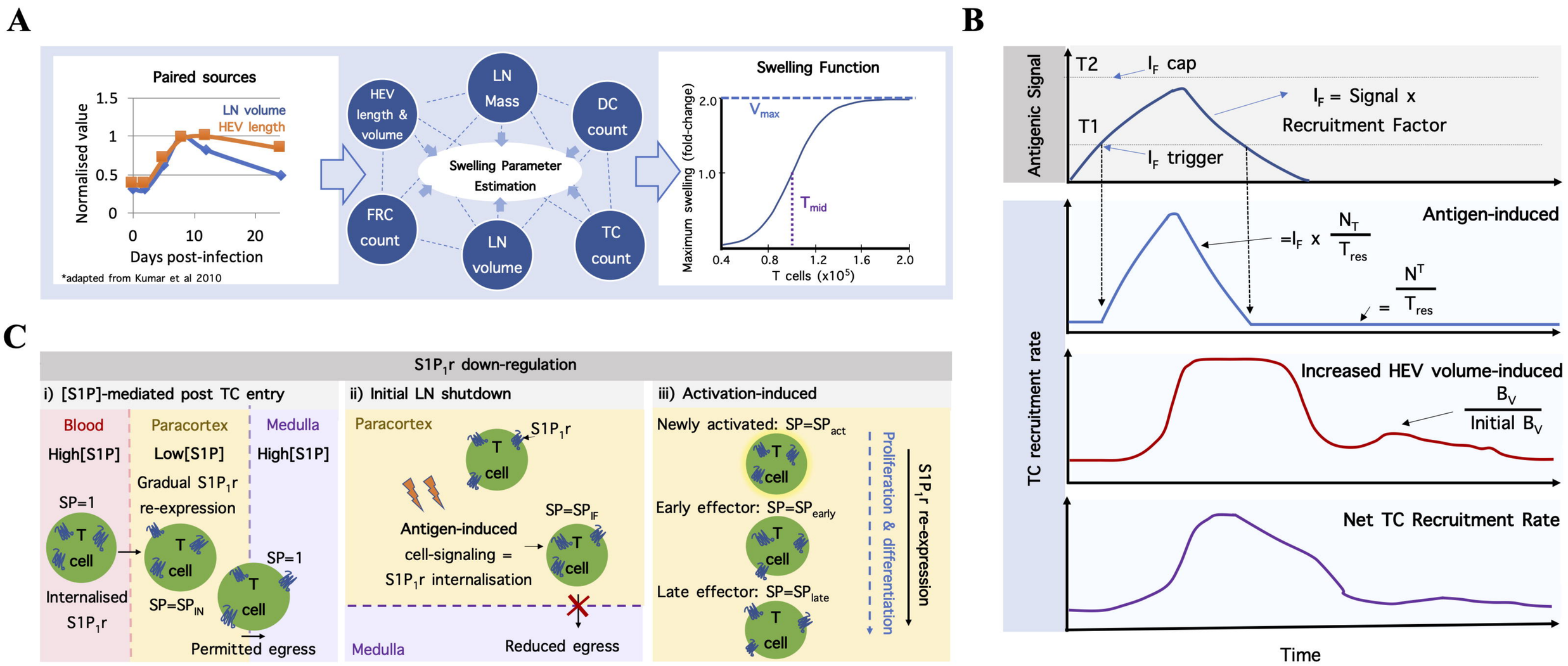

Figure 3: Structure of the code to set up and run the model. A) The model is initiated in the absence of stimulus, then capacity for paracortical volume change is introduced and variables storing initial starting volumes are updated. Cells (TCs and DCs) are represented by agents that store information about interaction history and present state. The 'Context' describes the environment and 'Projections' between agents allow information transfer. Each time-step represents 20s and model outputs are recorded every, 1, 15 or 180 time-steps. B) Following equilibration, the 'main' function calls a repeated series of sub-functions that describe DC arrival and TC response. Each function contains further actions, with descriptions available within the supplementary (S3 File).

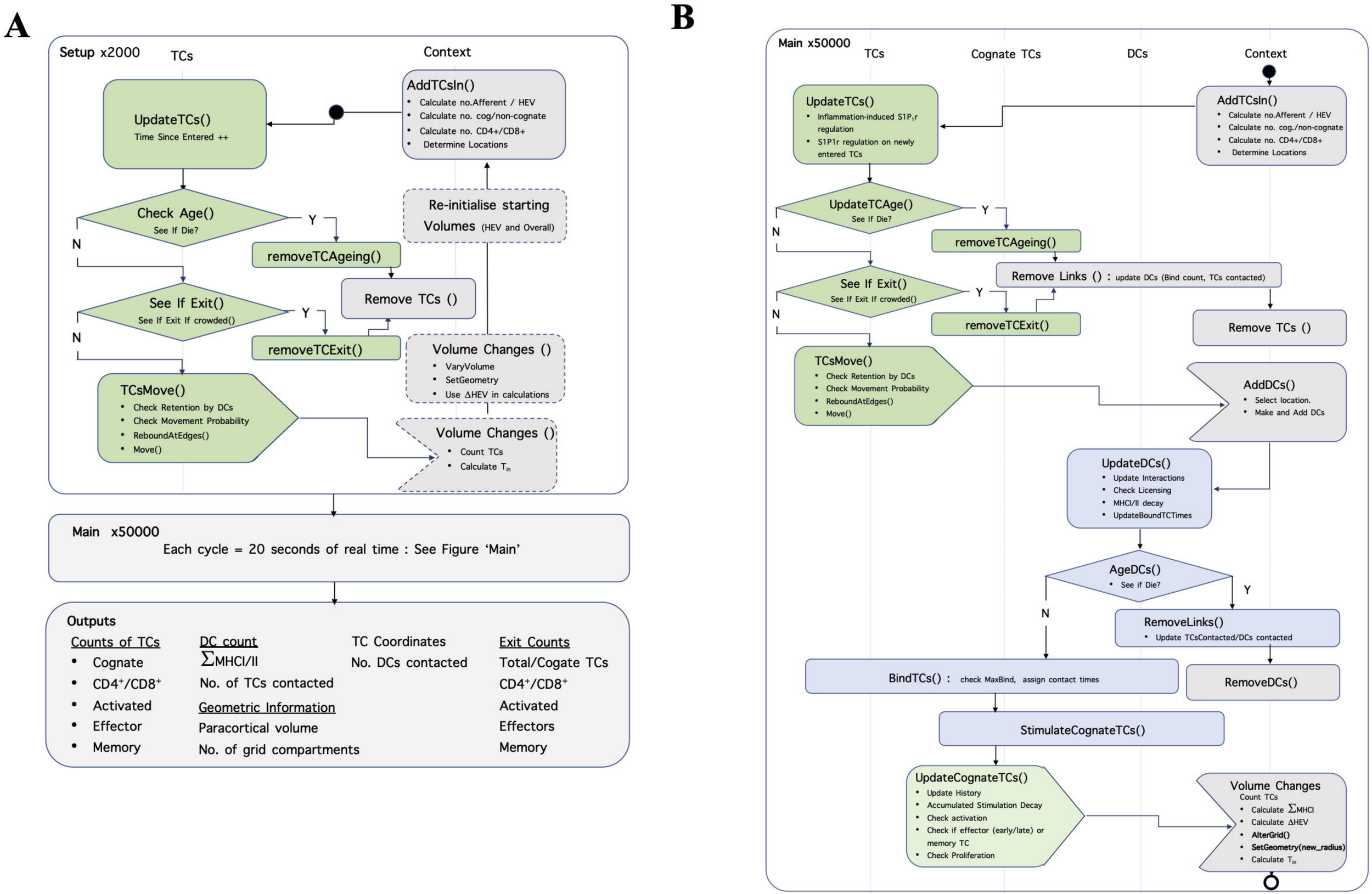

Figure 4: Model visualization. A) The environment is divided into grid compartments and in this case, the TCs are color-coded based on time spent in the paracortex. B) The grid (cubes with sides of 6μm) is used to distinguish the neighboring areas of cells and cell migration.

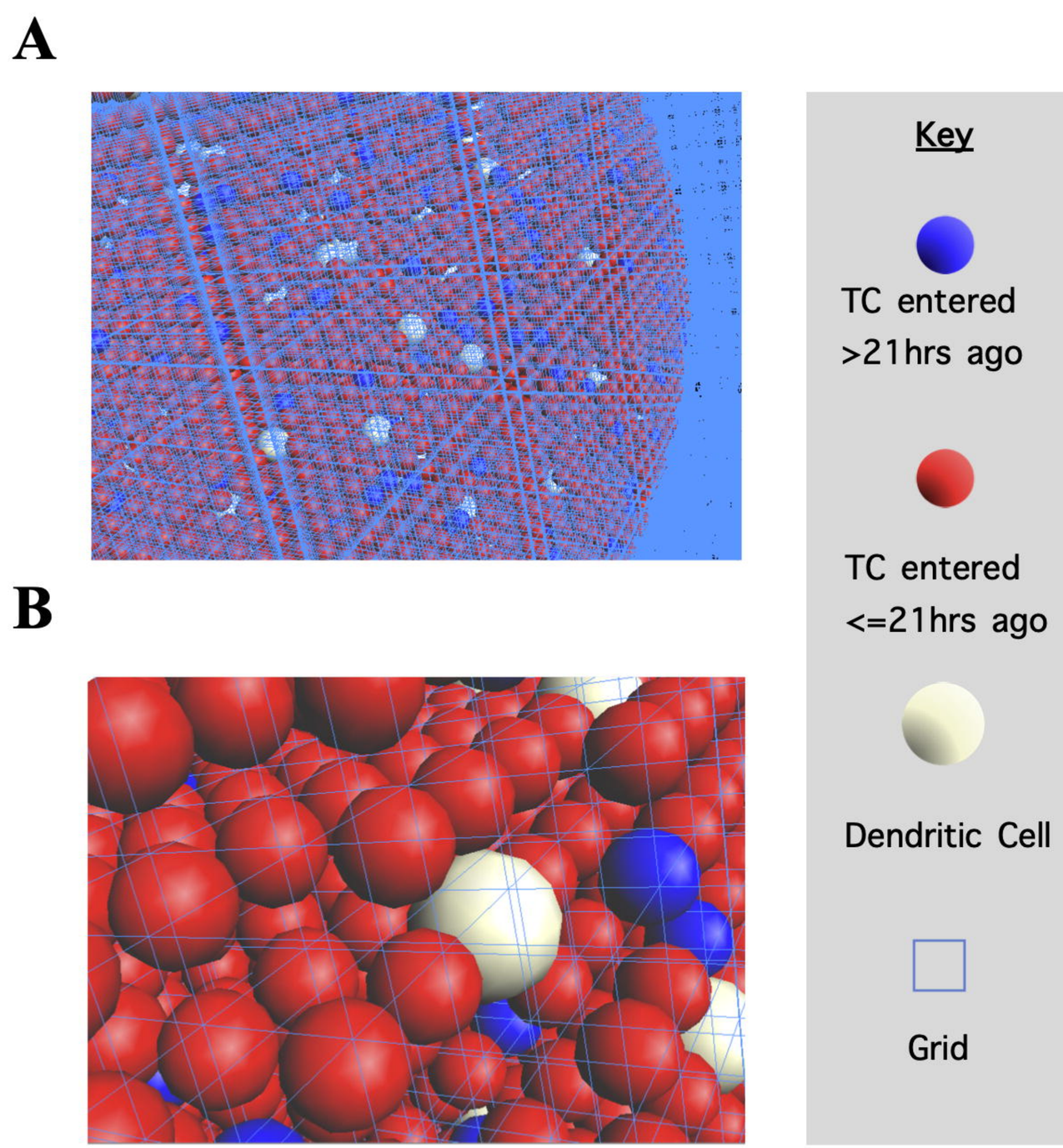

Figure 5. Baseline TC motility. A) TC tracking through the paracortex with individual tracks displayed. TCs entered centrally, representing entry from HEVs, and at the top of the paracortex, representing entry in afferent lymph (yellow arrow). TCs exited at the periphery (green arrows). B) Tracks of 200 TCs (each colour represents one TC path) transposed to the same origin point display the random walk behaviour outwards from the origin. C) Most TCs completed transit in <24hrs. D) Mean TC velocity over the entirety of their path. E) Mean and SEM (n=100) of TC displacement from entry point. F) Mean (+/-SEM) of TC displacement showed a linear relationship to the square root of time, indicating that random walk behaviour is maintained.

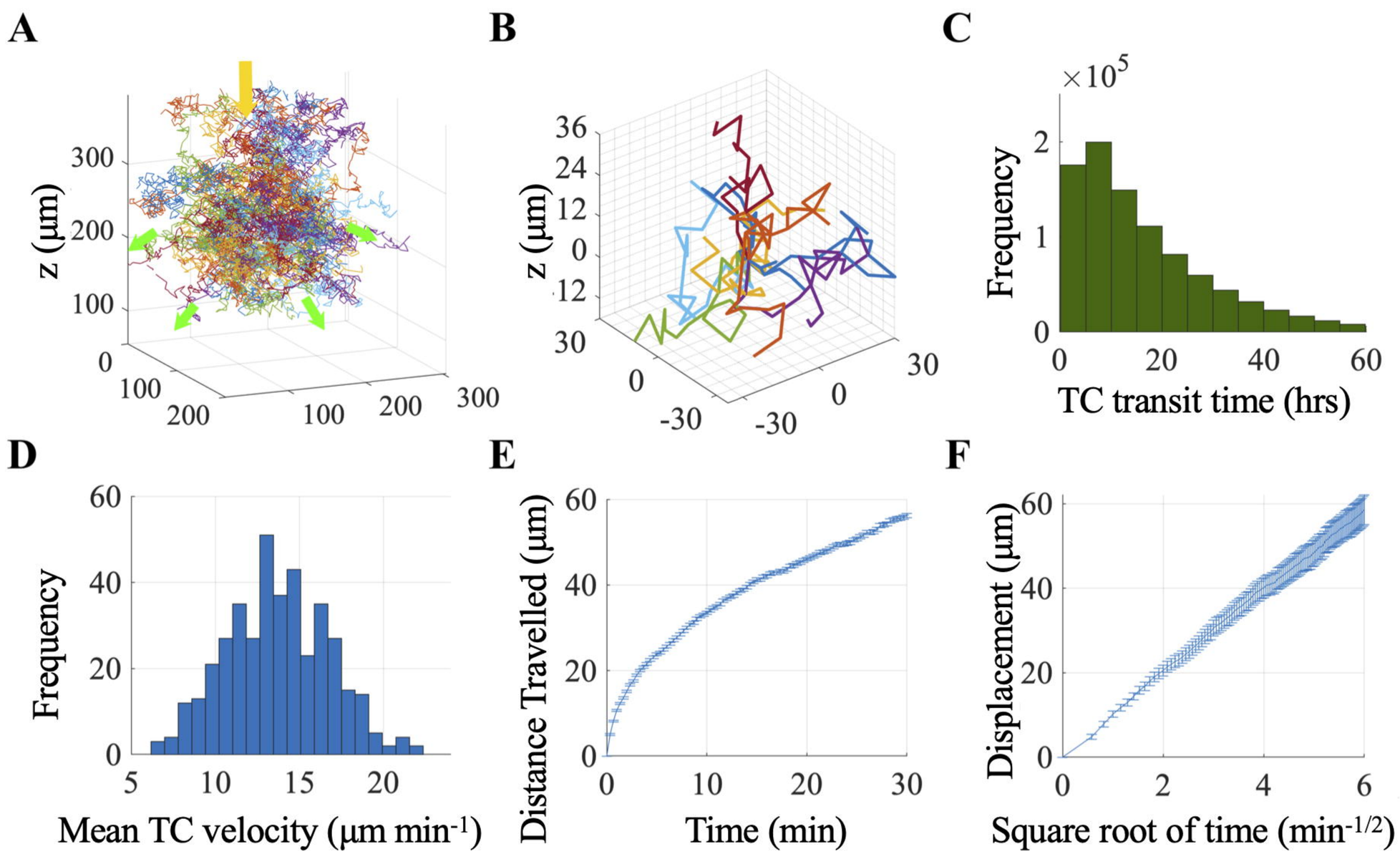

Figure 6. TC responses in the paracortex following entry of agDCs under baseline conditions. Average result with SEM of 12 simulations. Note the differing vertical scales. Incoming agDCs numbers are depicted by the dot-dashed line in B (right axis). The total number of TCs (black line in A) peaked in the paracortex at 3.5 days and was comprised mainly of non-cognate naïve TCs, as the number of effector TCs (blue line A) peaked at day 6. The appearance of activated TCs (red line in B) began 12 hours after the first agDCs entered. Memory TCs (black line in B) began to appear at 5 days and 25% of the peak number of memory TCs remained at the end of the simulation. Cognate CD4$^+$ TCs (Green line in C) began to proliferate extensively at day 2.2. Cognate CD8$^+$ TCs (purple line C) began to proliferate at day 4 and reached numbers 10x more than cognate CD4$^+$ TCs. D) TC entry rate increased 2x, peaking at day 3, whilst TC egress rate declined between day 1 and 2, then increased 3x by day 4.

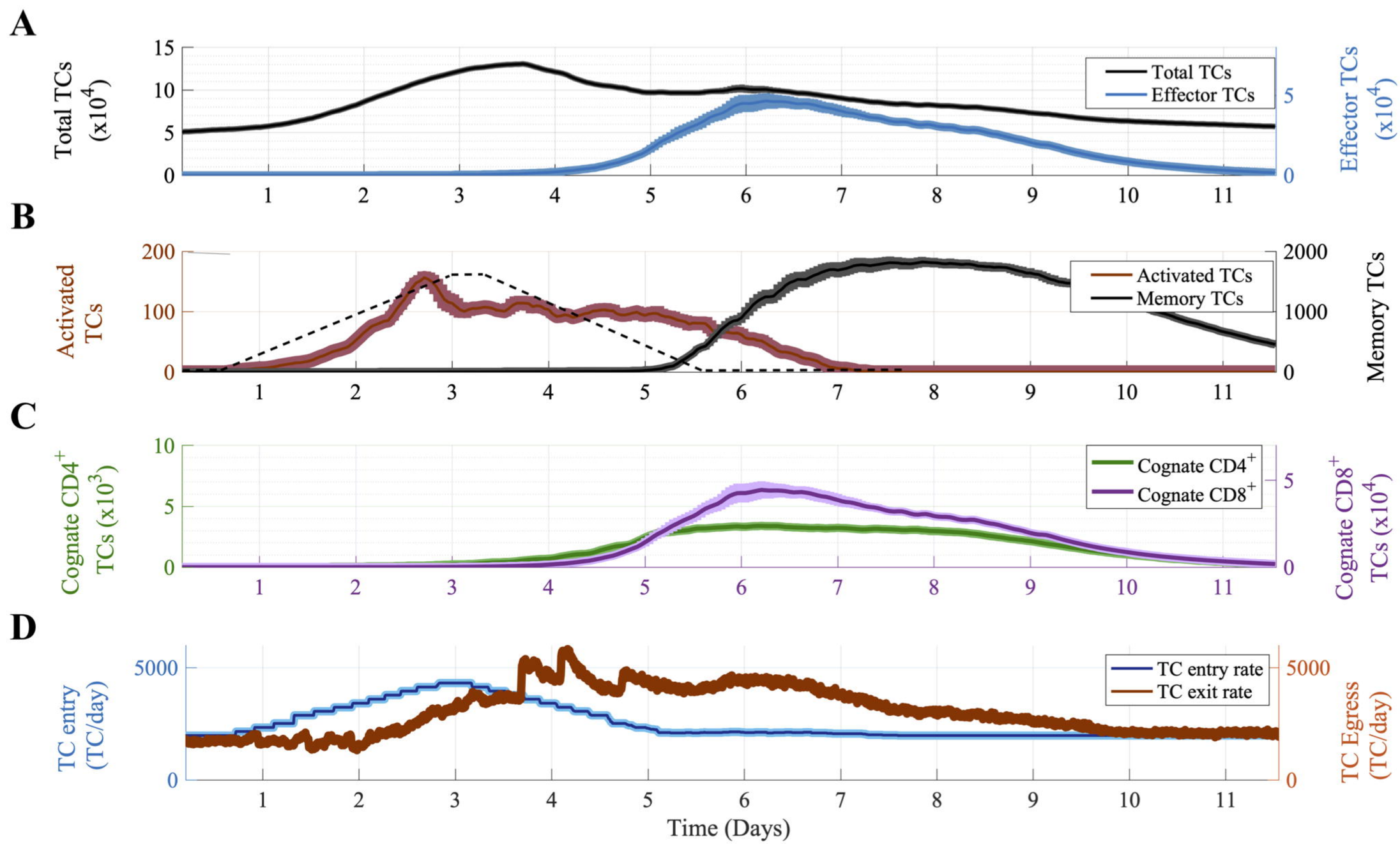

Figure 7. Comparison between in vivo assessments of the effects of $S1P_1r$ downregulation and model predictions. Top row contains experimental data, and bottom row shows comparable modelling results. A. Pre-activated wildtype TCs ($S1P_1r$) and TCs over-expressing $S1P_1r$ ($S1P_1r$++) were transferred into mice and further TC entry was blocked. After 15 hours there was a 90% reduction in retention of $S1P_1r$++ activated TCs. Adapted from Lo *et al* 2005. B) Activated TC number in the LNs 24 hrs post-transfer dropped by 40% in transgenic mice with constitutive $S1P_1r$ expression while (C) proliferative $CD4^+$ and $CD8^+$ TC response decreased to 20% & 6% of that of the wild-type mice. Adapted from Gräler *et al* 1997. D-F). The results of simulations (n=10) preventing $S1P_1r$ downregulation (-SP regulation) compared to baseline simulations (+SP regulation) showed similar trends to these *in-vivo* results (which were not used in model construction). Mean (+-SEM) total activated TCs number was reduced 60%, 72% and 81% at V_{max}=1.2,1.5 & 2. E) The mean (+-SEM) total $CD8^+$ TC number, was diminished to 25,15 and 18% of control response at V_{max}=1.2,1.5 & 2. F) $CD4^+$ TC number was similarly diminished to 8-10% of control at all V_{max} values.

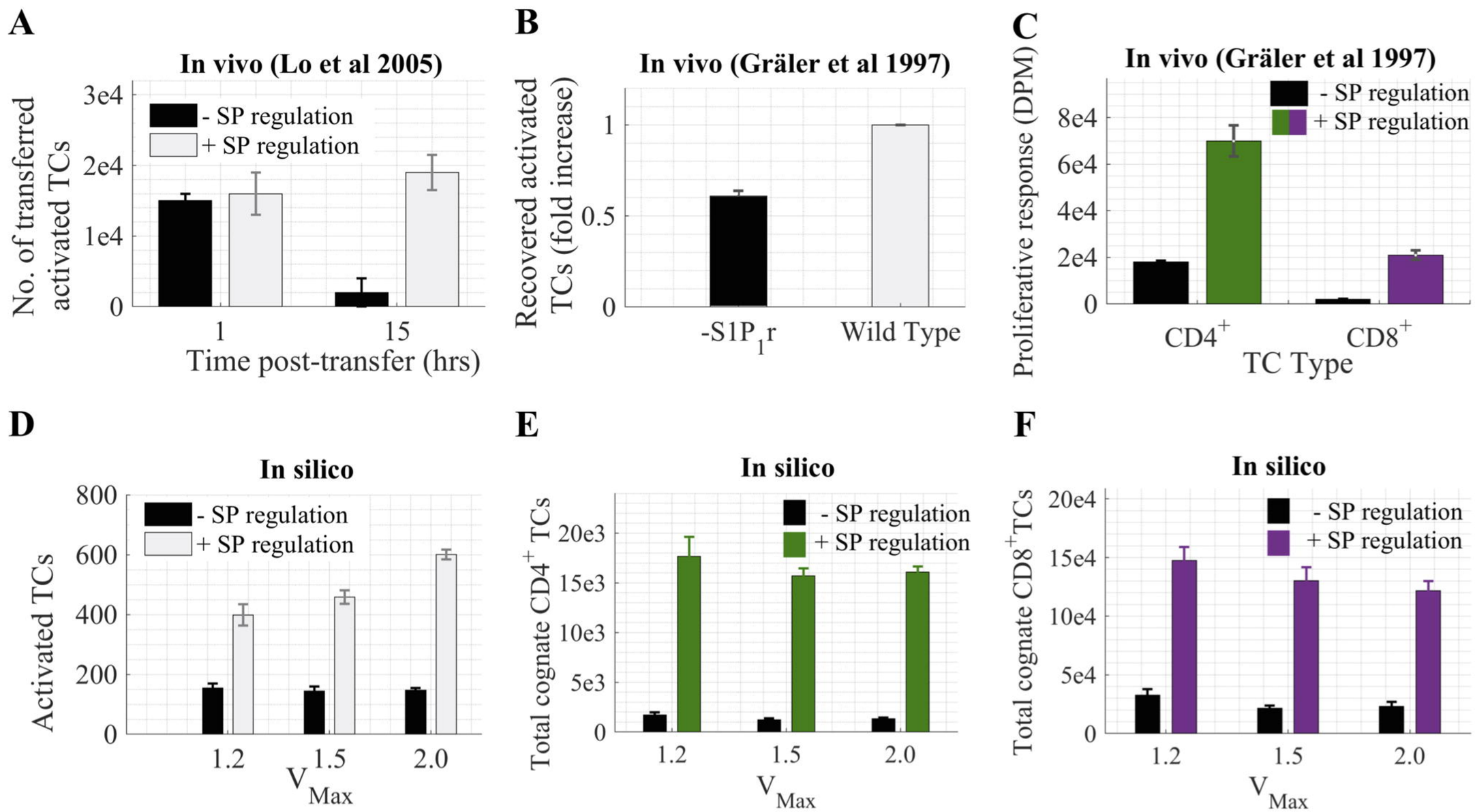

Figure 8. The variation in TC subsets as V_{max} was varied from 1 to 2.8 with $T_{mid}=10^5$. A) The total activated number of TCs in the paracortex incrementally increased with V_{max} and doubled in number between $V_{max}=1$ and 2.8. ($R^2= 0.96$, $p=1.07\times10^{-6}$). B) The total number of effector TCs decreased 0.3x with increasing V_{max} ($R^2=0.86$, $p=1.23\times10^{-4}$). C) The total number of cognate $CD4^+$ TCs that exited positively correlated with V_{max} ($R^2=0.76$, $p=0.001$) and increased 1.3x. D) The total cognate $CD8^+$ TCs negatively correlated with V_{max} ($R^2=0.855$, $p=1.28\times10^{-4}$). E,F) Peak entry and peak exit rate increased proportionally to V_{max}. All results are the mean of $n\geq7$ simulations with SEM displayed.

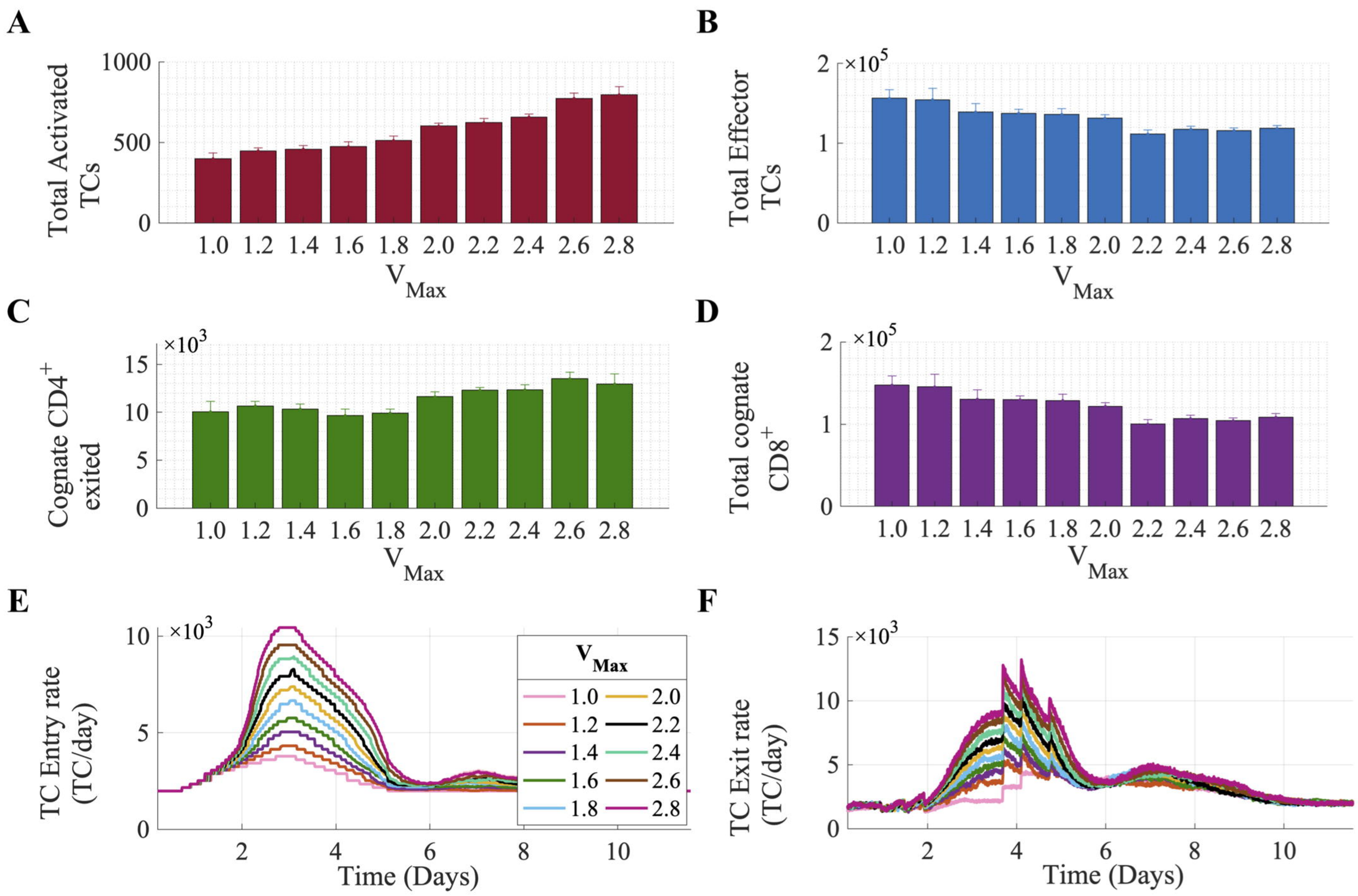

Figure 9. Increasing T_{mid} counteracts the loss in effector TCs with V_{max}. Swelling was varied with $T_{mid}=8x10^4$ and $T_{mid}=1.3x10^5$ instead of default (Figure 8) . A) The paracortex swells earlier and for a longer duration with a low T_{mid}. B) TC activation increased with larger swelling, but a higher T_{mid} also reduced activation at a large swelling (p=0.002). C) With a lower T_{mid}, as swelling increased, effector TC number decreased. This effect was due to a change in $CD8^+$ TC number (D) as $CD4^+$ TC number (E) increased with V_{max} but was unaffected by varying T_{mid}. F) The results of simulations varying V_{max} in 0.2 increments with a higher T_{mid} of $1.2x10^5$ instead of baseline 10^5, eliminated the negative correlation between effector TCs and swelling. (G) Further simulations varying T_{mid} confirmed that at a large swelling (V_{max}=2.5), delayed swelling with a higher T_{mid} resulted in more total effectors TCs (R^2=0.97,p= $3x10^{-4}$).

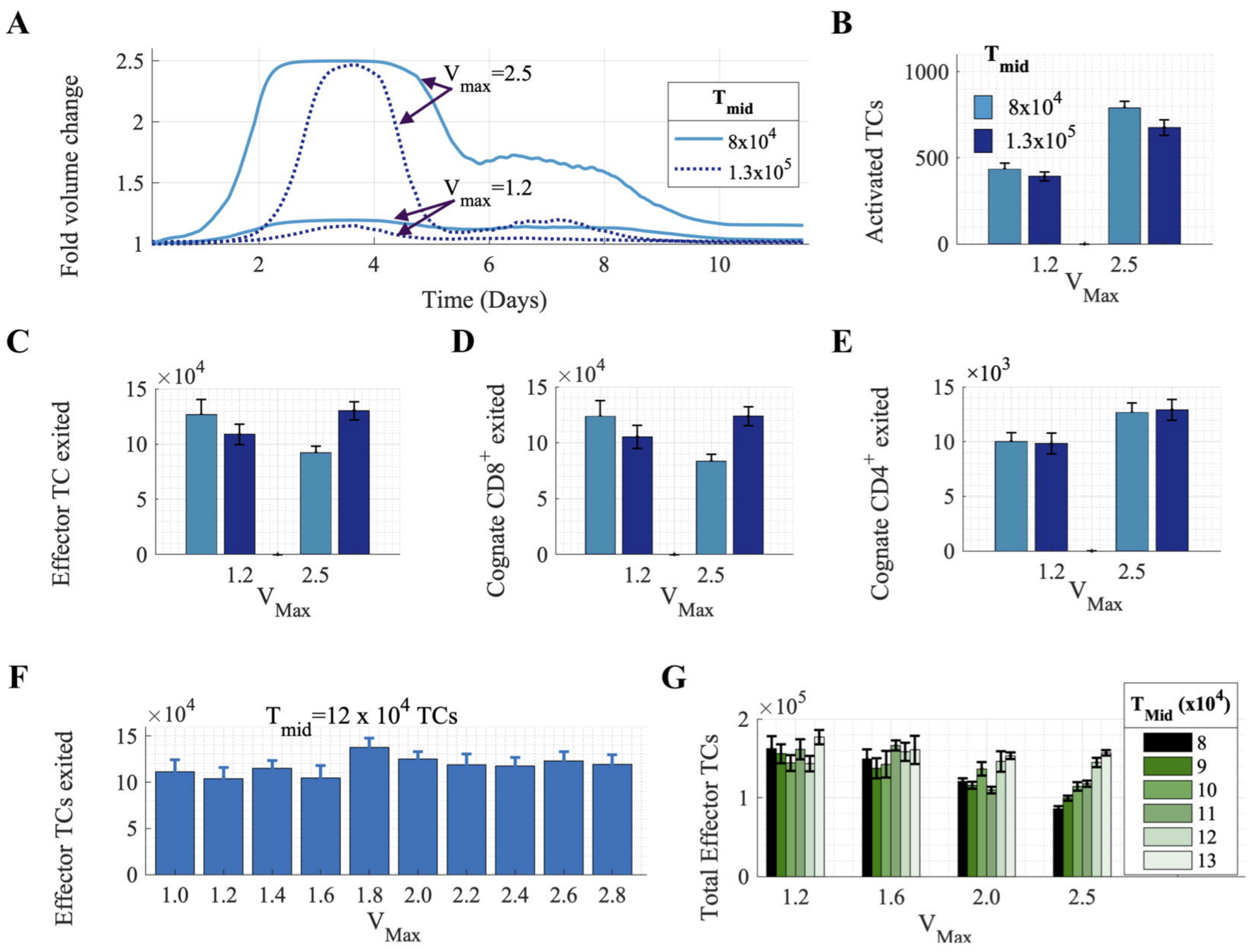

Figure 10. Changes in cognate TCs and agDC interaction with varying swelling. The mean number of interactions with agDCs recorded from cognate TCs present at day 3; (A) showed no trend with swelling, (B) showed no trend with swelling when taking into account the time spent by the TC in the paracortex and (C) showed no trend with T_{mid} when swelling was held constant. The mean number of cognate TCs that a DC interacted with during its lifespan was recorded, and the DCs grouped dependent on entry time (first 25% (Quartile 1) etc. to enter). With default T_{mid} of 10^5 (D), a very weak negative trend with swelling occurred during Quartile 1 (R^2=0.48, p=0.05), that became stronger the later the DC entered (R^2=0.69, p=0.002; R^2=0.77, p=6.9x10^{-4}; R^2=0.83, p=2.3x10^{-4} for quartile 2, 3 and 4 respectively). (E) With a higher T_{mid} of 1.2x10^5, no clear trend with swelling was identified. F) Only at a large swelling did DCs that entered later (Quartile 4) contact more cognate TCs when increasing T_{mid} (R^2=0.72, p=0.03).

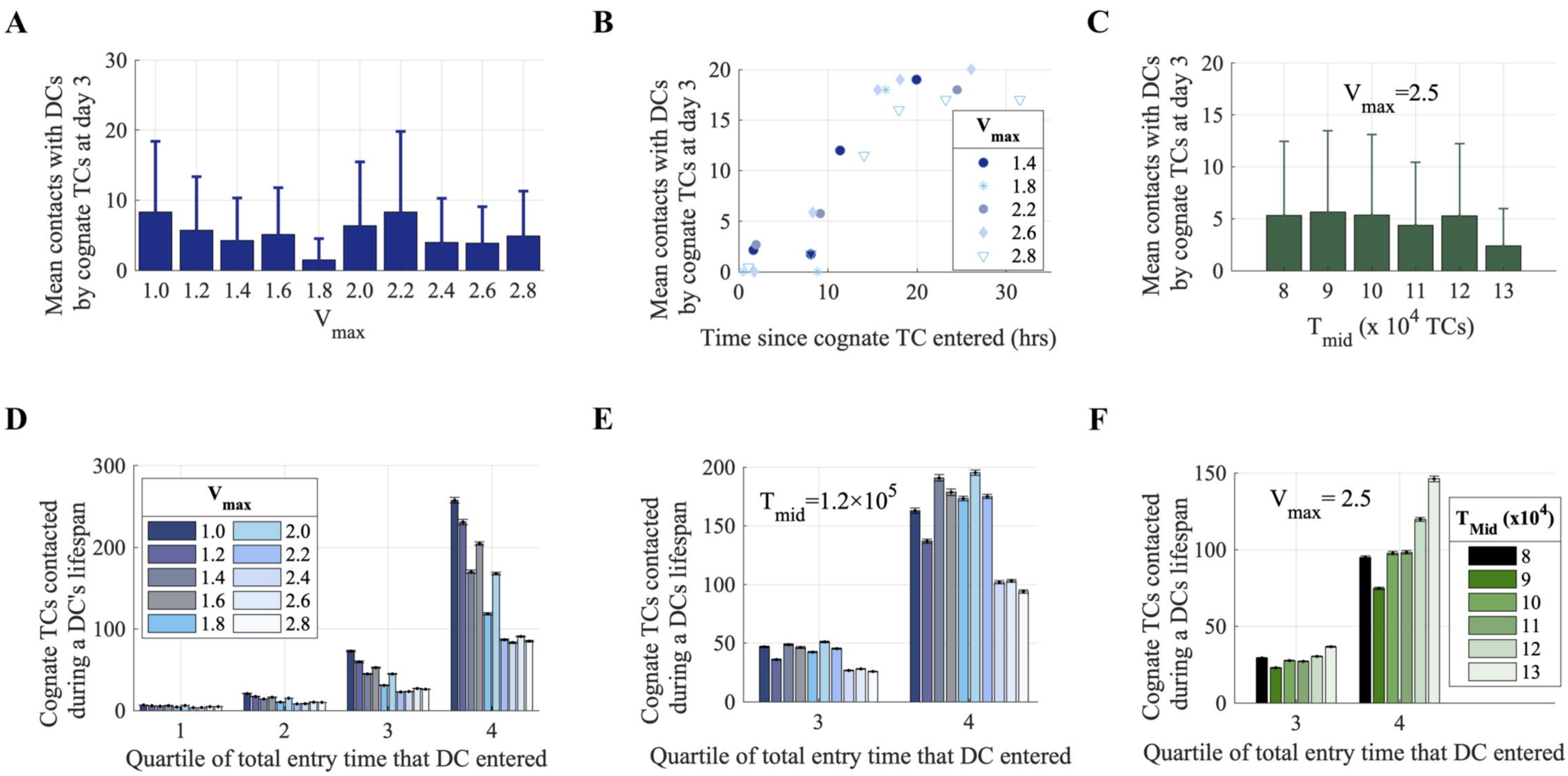

Figure 11. Temporary retention of effector TCs by modulating $S1P_1r$ expression on newly differentiated TCs (SP_{early}). A) Reducing SP_{early} resulted in a higher total number of TCs in the paracortex. B) Effector TCs that exited the paracortex were influenced more by SP_{early} than by V_{max}, negatively correlating with SP_{early} (R^2>=0.92, p<0.005). SP_{early} negatively correlated with both (C) $CD8^+$ TCs exited (R^2>0.92, p<0.005) and (D) $CD4^+$ TCs exited (R^2>0.91, p<0.005). E). The mean number of cognate TCs contacted increased as SP_{early} was lowered to 0.1 at each value of V_{max} but overall decreased with V_{max}. F) At a smaller maximal swelling, a higher TC to grid ratio was maintained but this did not translate to more or less effector TC production. (G) Reduced SP_{early} resulted in higher overall rates of TC egress in week 2 of the simulation.

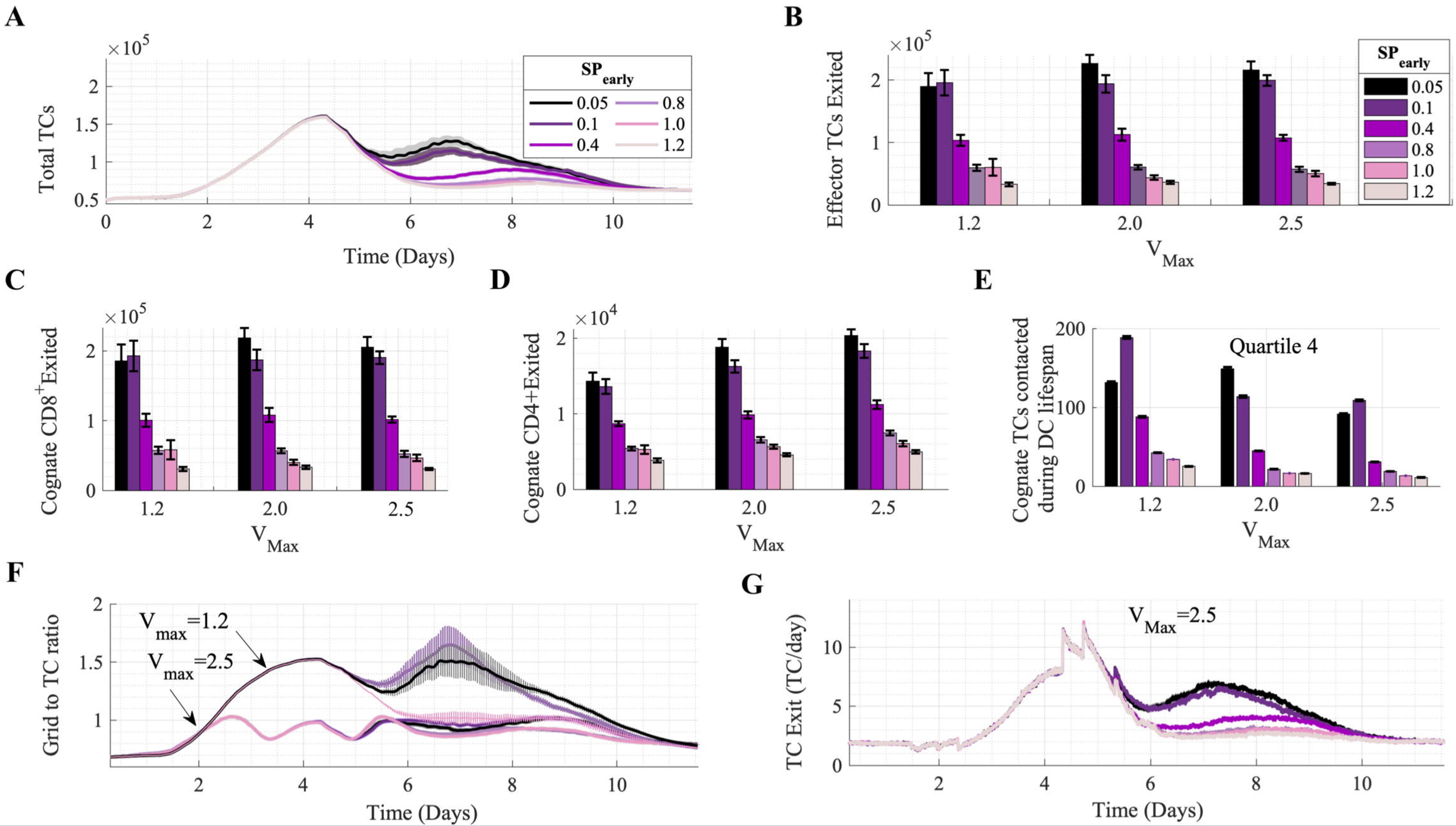
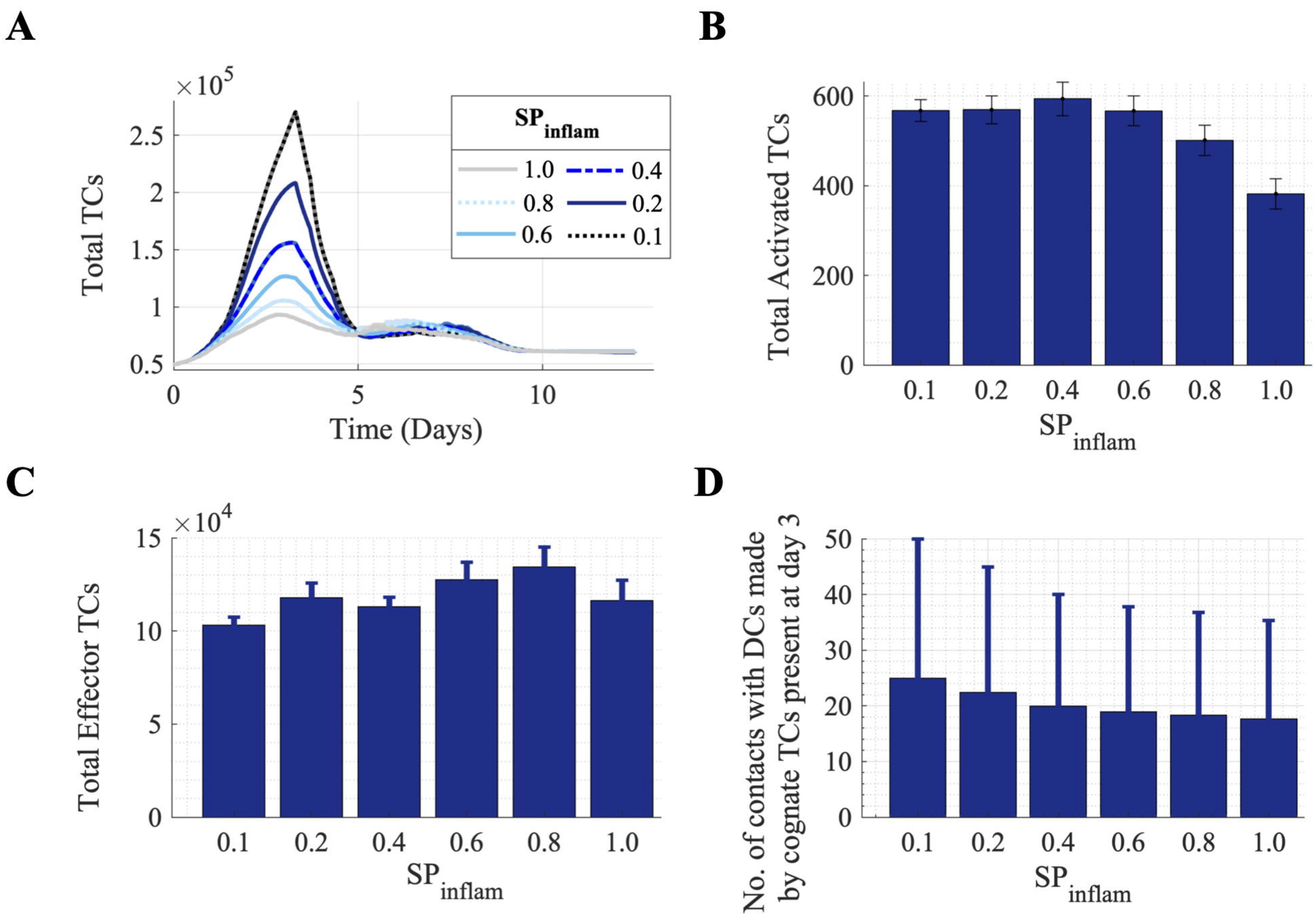
Figure 12. Varying LN shutdown by modulating inflammation-induced $S1P_1r$ downregulation (SP_{inflam}). Modulation of $S1P_1r$ down-regulation in response to initial detection of inflammatory signals from no downregulation (SP_{inflam}=1) to 90% downregulation (SP_{inflam}=0.1), A) total TC number decreases several fold but (B) TC activation increases (R^2= 0.83, p=0.01) while (C) Effector TC production shows no trend. D) Non-cognate TCs contact more DCs as SP_{inflam} is increased (R^2=0.93, p=1.7×10^{-3}).